Limb motion dictates how motor learning arises from arbitrary environmental dynamics

Gary C. Sing, Simon P. Orozco and Maurice A. Smith

J Neurophysiol 109:2466-2482, 2013. First published 30 January 2013;
doi: 10.1152/jn.00497.2011

You might find this additional info useful...

Supplementary material for this article can be found at:
http://jn.physiology.org/http://jn.physiology.org/content/suppl/2013/04/11/jn.00497.2011.DC1.html

This article cites 61 articles, 40 of which you can access for free at:
http://jn.physiology.org/content/109/10/2466.full#ref-list-1

This article has been cited by 1 other HighWire-hosted articles:
http://jn.physiology.org/content/109/10/2466#cited-by

Updated information and services including high resolution figures, can be found at:
http://jn.physiology.org/content/109/10/2466.full

Additional material and information about ***Journal of Neurophysiology*** can be found at:
http://www.the-aps.org/publications/jn

This information is current as of July 1, 2013.

Journal of Neurophysiology publishes original articles on the function of the nervous system. It is published 24 times a year (twice monthly) by the American Physiological Society, 9650 Rockville Pike, Bethesda MD 20814-3991. Copyright © 2013 the American Physiological Society. ESSN: 1522-1598. Visit our website at http://www.the-aps.org/.

Downloaded from http://jn.physiology.org/ at Harvard Univ on July 1, 2013

J Neurophysiol 109: 2466–2482, 2013.
First published January 30, 2013; doi:10.1152/jn.00497.2011.

Limb motion dictates how motor learning arises from arbitrary environmental dynamics

Gary C. Sing, Simon P. Orozco, and Maurice A. Smith
Center for Brain Science, Harvard School of Engineering and Applied Sciences, Cambridge, Massachusetts

Submitted 3 June 2011; accepted in final form 28 January 2013

Sing GC, Orozco SP, Smith MA. Limb motion dictates how motor learning arises from arbitrary environmental dynamics. *J Neurophysiol* 109: 2466–2482, 2013. First published January 30, 2013; doi:10.1152/jn.00497.2011.—A key idea in motor learning is that internal models of environmental dynamics are internally represented as functions of spatial variables including position, velocity, and acceleration of body motion. We refer to such a representation as motion dependent. The evidence for a motion-dependent representation is, however, primarily based on examination of the adaptation to motion-dependent dynamic environments. To more rigorously test this idea, we examined the adaptive response to perturbations that cannot be well approximated by motion-state: force-impulses—brief, high-amplitude pulses of force. The induced adaptation characterizes the impulse response of the system—a widely used technique for probing system dynamics in engineering systems identification. Here we examined the adaptive responses to two different force-impulse perturbations during human voluntary reaching movements. We found that although neither could be well approximated by motion-state ($R^2 < 0.18$ in both cases), both perturbations induced single-trial adaptive responses that were ($R^2 > 0.87$). Moreover, these responses were similar in shape to those induced by low-fidelity motion-based approximations of the force-impulses ($r > 0.88$). Remarkably, we found that the motion dependence of the adaptive responses to force-impulses persisted, even after prolonged exposure ($R^2 > 0.95$). During a 300-trial training period, trial-to-trial fluctuations in the position, velocity, and acceleration of motion accurately predicted trial-to-trial fluctuations in the adaptive response, and the adaptation gradually became more specific to the perturbation, but only via reorganization of the structure of the motion-dependent representation. These results indicate that internal models of environmental dynamics represent these dynamics in a motion-dependent manner, regardless of the nature of the dynamics encountered.

motor adaptation; force pulse; motor primitives; force-field adaptation

PREVIOUS WORK HAS SHOWN that the human motor system learns to associate external force perturbations with the motion-state of the limb (i.e., the kinematic variables describing limb posture and motion, such as position, velocity, and acceleration) rather than with the times at which they occur (Conditt et al. 1997; Conditt and Mussa-Ivaldi 1999). Even discrete actions like button presses are consistently associated with motion-state rather than with time (Diedrichsen et al. 2007). This motion dependence can arise if adaptation is mediated by a population of motion-dependent motor primitives (Hwang et al. 2003; Mussa-Ivaldi and Bizzi 2000; Sing et al. 2009; Thoroughman and Shadmehr 2000; Thoroughman and Taylor 2005). In general, models based on motor primitives combine the contributions from a population of primitive elements to produce motor output (Poggio and Bizzi 2004) as a weighted sum of the contributions from individual primitive elements that have different activation functions. In this framework, adaptation arises by adapting the strengths of the individual contributions rather than by changing how each element is tuned. This adaptation proceeds in such a way as to result in a decrease in the error between the actual and desired motor outputs (Thoroughman and Shadmehr 2000).

A number of studies have demonstrated that motion-dependent dynamics that reflect or resemble the velocity of motion (Conditt et al. 1997; Conditt and Mussa-Ivaldi 1999), position (Sing et al. 2009), acceleration (Hwang et al. 2006), or combinations of position and velocity (Hwang et al. 2003; Sing et al. 2009) all induce motion-dependent learning. However, the current evidence for motion-dependent adaptation comes from these studies in which the dynamics to be learned were themselves motion dependent. This begs the question of whether motion-dependent adaptation would be observed if dynamics that were largely non-motion dependent were trained instead. If the motor primitive population could produce both motion-dependent and non-motion-dependent adaptive responses, one might expect that dynamics based on motion-state would preferentially elicit motion-dependent responses that could overshadow non-motion-dependent contributions to the adaptive response. Thus a more definitive test of the idea that motor primitives primarily produce motion-dependent responses would be to study the adaptive responses to dynamics that cannot be well approximated by motion-state, in order to determine whether the motor primitives are merely capable of producing motion-dependent adaptive responses or are obligated to do so.

One type of non-motion-dependent dynamics is a force-impulse perturbation (Fine and Thoroughman 2006; Smith et al. 2000), a short-duration, high-strength pulse of force. In system identification, the fundamental relationship between input and output is often characterized with the so-called "impulse response" of a system, which refers to the output observed when an impulse function is given for the input. An impulse is a particularly attractive stimulus for system identification because it is time limited and has a flat power spectral density, meaning that it provides equal excitation at all temporal frequencies. It is currently unknown how human motor adaptation responds to such a broad excitation across the frequency spectrum in terms of the feedforward changes in motor output. For linear systems the impulse response can fully characterize a system's input/output relationship (Bellman and Åström 1970), and in nonlinear system identification the impulse response generally serves as a starting point for such characterization (Friston et al. 1998; Koop et al. 1996). Consequently, in engineering systems analysis, determination of

Address for reprint requests and other correspondence: M. A. Smith, Harvard School of Engineering and Applied Sciences, Center for Brain Science, 60 Oxford St., Rm. 402, Cambridge, MA 02138 (e-mail: mas@seas.harvard.edu).

0022-3077/13 Copyright © 2013 the American Physiological Society

Downloaded from http://jn.physiology.org/ at Harvard Univ on July 1, 2013

the impulse response is generally the very first step in studying a system's behavior. In line with this idea, spike-triggered averaging, a technique for estimating the impulse response to neural spikes, has been widely used in investigations of the input/output relationships of cortically driven muscles (Cheney and Fetz 1984) and pyramidal tract cells in motor cortex (Kang et al. 1988), for example. However, the force patterns that constitute the impulse response for sensorimotor adaptation have not been previously measured.

Previous work has looked at the motion aftereffects induced by single-trial motor adaptation following brief force-impulse perturbations, which are highly non-motion dependent, in order to determine the impulse response for motor learning (Fine and Thoroughman 2006). This work found that force pulses (FPs) applied at very different positions during reaching arm movements (20–70% of the target distance) induced essentially identical motion aftereffects in the next movement, even though the kinematic trajectories during the pulsed movements varied widely, depending on the pulse onset location. However, since the motions observed on aftereffect trials depend on a variety of factors, including feedforward force patterns, hand speed, feedback control gains, and limb stiffness, viscosity, and inertia (Bhushan and Shadmehr 1999), it is difficult to determine what feedforward motor output pattern leads to any particular aftereffect motion. The authors were thus unable to determine the temporal structure of the response dynamics. Consequently, the fundamental relationship between the dynamics of the perturbation and the dynamics of the adaptive response is not yet understood.

Are adaptive responses dominated by motion-dependent components even when perturbations that do not resemble any of these components drive the adaptation? Here, we designed experiments in which we delivered brief force-impulse perturbations and directly measured the corresponding adaptive changes in motor output to gain insight into the nature of the primitives underlying motor adaptation. In *experiment 1* we determined the extent to which the adaptive responses to force-impulse perturbations reflected motion-dependent representations for motor output. In *experiment 2* we compared the adaptive responses elicited by force-impulse perturbations to those elicited by motion-dependent approximations of these perturbations that induced very different patterns of motor errors. In *experiment 3* we examined how the adaptive response to force-impulse perturbations evolves during extended training so that we could compare the adaptive changes from the earliest possible point in the learning curve (single-trial adaptation) to well after asymptote (300-trial adaptation) to determine the extent to which adaptive responses remain motion dependent as they grow and evolve with training.

MATERIALS AND METHODS

Participants. Thirty-eight healthy individuals (22 women, 16 men; median age: 19 yr, age range: 18–34 yr; all right-handed) participated in three different experiments. The subjects did not have prior knowledge of the experiment's purpose or prior exposure to force-field adaptation experiments. They also did not participate in multiple experiments, and all provided informed consent. All experimental protocols were approved by the Harvard University Institutional Review Board.

General task. Participants were asked to sit in front of a vertically mounted computer screen while grasping the handle of a two-joint robotic manipulandum in the *x*-*y* plane (Fig. 1*A*). The *xy*-position of the handle was indicated by the *xz*-position of a cursor (3 mm in diameter) on the computer screen. Subjects were instructed to make 500-ms, 10-cm reaching arm movements in the 90° (forward) and 270° (backward) directions from one circular target (1 cm in diameter) to another in as straight a line as possible. Depending on the experiment, subjects were perturbed either with force pulses (FPs) or motion-dependent force fields (FFs) that were equivalent to the FPs in a manner that is described below.

Force pulses. In *experiments 1* and *3* we applied force-impulse perturbations to the hand during the point-to-point reaching arm movements. These FPs were 18 N in magnitude and 80 ms in total duration (Fig. 1, *B* and *D*) and are described by the following equation:

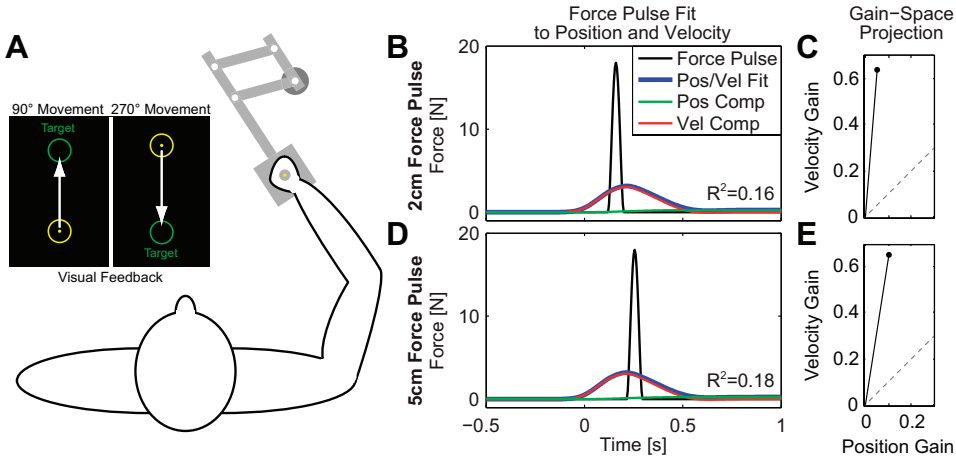


Fig. 1. Illustration of the experimental paradigm. *A*: subjects grasped the handle of a robotic manipulandum while making 10-cm, point-to-point reaching arm motions in the 90° and 270° directions. In *experiment 1*, movements were occasionally perturbed with different force pulses (FPs)—impulselike applications of force in the direction lateral to movement that were 18 N in magnitude and 80 ms in duration. Note that the actual target size (1 cm) is exaggerated here. *B* and *D*: these FPs were triggered at either the 2-cm (*B*) or 5-cm (*D*) point of the 10-cm movement. In *experiment 3*, the same 5-cm FP was consistently applied. The motion-dependent representations of the FPs (*Eq. 4*) are shown as the blue traces, with the individual subcomponents shown in green (the position component) and red (the velocity component). Note that these FPs are poorly characterized by position and velocity—R^2 values for the motion-dependent fits are at *bottom right*. *C* and *E*: the FPs can be represented as points in a 2D position/velocity gain-space, where the *x*- and *y*-coordinates correspond to the projection of the FP trace into the position/velocity subspace (see MATERIALS AND METHODS). These points represent the "equivalent" force fields (FFs) for the FPs. Note that the diagonal dashed lines represent $y = x$.

Downloaded from http://jn.physiology.org/ at Harvard Univ on July 1, 2013

$$F_{FP} = \frac{48}{5} \cdot \left(30\left((t - t_{onset}) / T_{FP}\right)^4 - 60\left((t - t_{onset}) / T_{FP}\right)^3 + 30\left((t - t_{onset}) / T_{FP}\right)^2\right),\ t_{onset} < t < T_{FP} + t_{onset} \quad (1)$$

These FPs have the same bell-curve shape as a minimum-jerk velocity profile because we used the same 4th-order polynomial (*Eq. 1*) to define the FP shape as the one that characterizes a minimum-jerk velocity profile for a point-to-point movement. t_{onset} in *Eq. 1* refers to the time at which the longitudinal position crosses either the 2 cm or 5 cm mark, and $T_{FP} = 80$ ms. They were applied in either the 0° (rightward) or 180° (leftward) direction, beginning at either 2 cm or 5 cm into the 10-cm reaching movement. Note that these two FPs were among those studied by Fine and Thoroughman (2006). The motor time constant for the manipulandum used in our study is 4.2 ms. The fidelity of the FP delivery is quite high given that this time constant is approximately 1/20th the duration of the FP perturbation. See Supplemental Fig. S1 for further analysis on the implementation of these FPs.[1]

Equivalent force fields. We hypothesized that the motor system effectively represents the non-motion-dependent FPs as "equivalent" motion-dependent FFs. We further hypothesized that the position- and velocity dependence of these equivalent FFs could be estimated by projecting the force vs. time traces of the FPs onto the average position and velocity traces we measured (Fig. 1, *B* and *D*). Specifically, we found the position dependence by projecting the FP shape onto the normalized position trace:

$$K = F(t) \cdot \frac{P(t)}{\|P(t)\|} \quad (2)$$

We then found the velocity dependence by projecting the FP shape onto the normalized velocity trace:

$$B = F(t) \cdot \frac{V(t)}{\|V(t)\|} \quad (3)$$

Thus the equivalent FFs were proportional to a linear combination of the position and velocity of the hand and were applied perpendicular to the reach direction like the FP perturbations they were based on. These FFs were described by the following equation:

$$\begin{bmatrix} F_x \\ F_y \end{bmatrix} = \begin{bmatrix} 0 & K \\ -K & 0 \end{bmatrix} \begin{bmatrix} x \\ y \end{bmatrix} + \begin{bmatrix} 0 & B \\ -B & 0 \end{bmatrix} \begin{bmatrix} \dot{x} \\ \dot{y} \end{bmatrix} \quad (4)$$

where $K = \pm 2.3$ N/m, $B = \pm 9.63$ Ns/m (FF equivalent to the 2-cm FP) or $K = \pm 4.6$ N/m, $B = \pm 9.8$ Ns/m (FF equivalent to the 5-cm FP). Note that x and y refer to hand position relative to the starting position and $\dot{x}$ and $\dot{y}$ refer to the hand velocity. In this equation, positive K and B values lead to forces that perturb the hand clockwise with respect to the direction of hand motion and negative values perturb the hand counterclockwise. These FFs can be represented in position/velocity gain-space as a point at [2.3 N/m, 9.63 Ns/m], for example. Here, we plot the representations of these FFs in normalized gain-space (Fig. 1, *C* and *E*), where [1,0] corresponds to $K = 45$ N/m, $B = 0$ Ns/m and [0,1] corresponds to $K = 0$ N/m, $B = 15$ Ns/m. This normalization is accomplished by dividing all position gains by 45 N/m and all velocity gains by 15 Ns/m. We chose to implement this normalization procedure to be consistent with previous work, which displayed adaptation to purely position-dependent ($K = 45$ N/m) and velocity-dependent ($B = 15$ Ns/m) FFs in the normalized position/velocity gain-space (Sing et al. 2009). This previous work chose to use these two FFs because the peak forces experienced are very similar (position-dependent FF: peak position of 10 cm multiplied by 45 N/m yields 4.5 N; velocity-dependent FF: peak velocity of 0.3 m/s multiplied by 15 Ns/m yields 4.5 N).

[1]Supplemental Material for this article is available online at the Journal website.

In the present work, we extend the gain-space analysis to include acceleration (see Figs. 4 and 6). A hypothetical acceleration-dependent FF would be of strength $M = 2.93$ Ns^2/m in order to produce a peak force of 4.5 N during 10-cm movements with peak accelerations of 1.51 m/s^2 (calculated from an average acceleration trace). We thus normalize the acceleration gains by 2.93 Ns^2/m in the normalized position/velocity/acceleration gain-space (see Fig. 4, *D–F*). The equivalent FF for the 5-cm FP can then be described as

$$\begin{bmatrix} F_x \\ F_y \end{bmatrix} = \begin{bmatrix} 0 & K \\ -K & 0 \end{bmatrix} \begin{bmatrix} x \\ y \end{bmatrix} + \begin{bmatrix} 0 & B \\ -B & 0 \end{bmatrix} \begin{bmatrix} \dot{x} \\ \dot{y} \end{bmatrix} + \begin{bmatrix} 0 & M \\ -M & 0 \end{bmatrix} \begin{bmatrix} \ddot{x} \\ \ddot{y} \end{bmatrix} \quad (5)$$

where $K = 2.3$ N/m, $B = 9.63$ Ns/m, and $M = -0.61$ Ns^2/m. Note that the acceleration component for the motion-dependent approximation of the FP is negative, and thus the acceleration component of the adaptation is also negative. In Fig. 4*D*, we use symbol size to graphically represent the magnitude of the acceleration component of this FF and the associated learning.

Error-clamp probe trials. We used error-clamp (EC) probe trials to measure the feedforward trial-to-trial adaptation induced by the perturbing FPs or equivalent FFs (Scheidt et al. 2000; Sing et al. 2009; Smith et al. 2006; Wagner and Smith 2008). Forces produced during learning can arise from several sources, such as predictive feedforward adaptation, within-trial online error feedback, cocontraction/stiffness factors, and passive dynamics. Although measuring the combined output is relatively straightforward, it is much more difficult to evaluate the trial-to-trial predictive adaptation because of masking by the other force contributions. During EC probe trials, subjects' arm reaches are forced to move in a straight line by a stiff spring/damper system ($K = 6$ kN/m, $B = 250$ Ns/m), and kinematic error within trial can largely be removed by restricting 99% of lateral errors to no more than 1.2 mm. These probe trials essentially eliminate the kinematic error that drives online error correction and the effects of stiffness. Thus by analyzing adaptive responses on EC trials rather than on the perturbation trials themselves, we avoid the issue of having perturbation (and the feedback response that it elicits) present in the data used to measure the adaptive response. Correspondingly, the passive dynamics and the limb motion on which these dynamics depend are not perturbed on the trials on which the adaptive response is assessed, allowing us to escape the issue of having to deal with nonlinearities that may arise when changes in passive dynamics and changes in feedforward control interact. The effects of passive dynamics can thus be canceled via baseline subtraction, as described below in the methods for the different experiments. This allows us to unmask the feedforward lateral force output, which is the opposite of the robot-clamping force. After extended exposure to motion-dependent FFs, the motor output measured during these EC trials closely resembles the ideal compensatory force patterns for the different FFs in both magnitude and shape (Sing et al. 2009), indicating that EC probe trials enable accurate measurement of feedforward output.

Experiment 1: single-trial adaptation to FPs. The motivation for this experiment was to measure the motor system's adaptive response to non-motion-dependent FPs. Eighteen subjects (9 women, 9 men; median age: 20.5 yr, age range: 18–25 yr; all right-handed) participated in this experiment. *Experiment 1* consisted of 1,922 trials. In the first 300 trials (150 each in the forward and backward directions), subjects gained familiarity with the basic point-to-point movement task before being subjected to the FP perturbations. In the following 1,622 movements, FPs were occasionally delivered during movement, with at most one FP per trial. A total of 192 FP trials were administered at a frequency of ~1 perturbation per 8.5 trials. These FP trials were equally divided between the two movement directions (forward and back), two perturbation directions (leftward and rightward), and two FP onset locations (2 cm and 5 cm into the movement) such that 24 perturbations of each possible type were delivered during the course of the experiment.

Downloaded from http://jn.physiology.org/ at Harvard Univ on July 1, 2013

To measure the single-trial adaptation resulting from each FP perturbation, we sandwiched each FP trial between two EC trials in the same movement direction. This allowed us to estimate the single-trial adaptation to the FP in each "triplet" (EC-FP-EC) by taking the difference between the lateral force patterns measured during the post-FP and pre-FP EC trials. This measurement allows us to isolate any learning-related changes while removing contributions from baseline passive dynamics. After each triplet, we washed out any adaptation with three to five null-field washout trials. Triplets in the backward direction were always interleaved with triplets in the forward direction, leading to six-trial groupings with the following structure: $EC_{backward}$-$EC_{forward}$-$FP_{backward}$-$FP_{forward}$-$EC_{backward}$-$EC_{forward}$. The experiment was divided into 19 blocks of ~100 trials each, with 1-min breaks between blocks. Subject-average perturbed hand paths were calculated for each FP type for each movement direction and were then combined together for the population averages (Figs. 2 and 3). Subject-average single-trial adaptive responses were calculated for each FP type across movement and pulse directions with appropriate rectification (i.e., adaptive responses to the backward-leftward and forward-rightward pulses were combined with the negative responses to the backward-rightward and forward-leftward pulses) and were then combined together for the population averages (Figs. 2 and 3).

Experiment 2: single-trial adaptation to equivalent FFs. The motivation for this second experiment was to see whether the motor system adapted to the FPs as their equivalent motion-dependent FFs. Twelve subjects (6 women, 6 men; median age: 18 yr, age range: 18–25 yr; all right-handed) participated in this experiment. The experimental structure was identical to *experiment 1*, except that the equivalent FFs described above were substituted for the FP perturbations. Subject-average perturbed hand paths were calculated for each FF for each direction and were then combined together for the population averages (Fig. 3). Subject-average single-trial adaptive responses were calculated for each FF across movement and FF directions with appropriate rectification and were then combined together for the population averages (Fig. 3).

Experiment 3: extended exposure to FPs. The motivation for this third experiment was to see whether the motion dependence of the adaptive responses to the FPs disappeared with extended training. Eight subjects (7 women, 1 man; median age: 19.5 yr, age range: 18–34 yr; all right-handed) participated in this experiment. The experiment began with a 600-trial baseline period in which no perturbations were applied. This block consisted of 300 trials each in the forward and backward directions, and the baseline period was split up into 6 sets of 100 trials each. These 600 trials were composed of 412 null-field trials and 188 EC trials, randomly intermixed. Subjects were then exposed to a block of consecutive 5-cm FPs in the backward direction to either the left (4 subjects) or right (4 subjects). This block, which allowed for extended learning of these 5-cm FPs, consisted of 392 trials in total: 300 FP trials and 92 pseudorandomly intermixed EC measurement trials (~23% of the trials). The experiment then concluded with 100 consecutive EC trials in the backward direction to measure the decay of the FP adaptation. All postfamiliarization trials in the forward direction were EC trials. All force patterns measured in the postfamiliarization period (i.e., learning and decay) were baseline subtracted, where the baseline was the average force pattern measured during the last 120 trials before learning onset (20 EC trials). This baseline subtraction was performed to remove any component of the motor output that is not produced in response to the FP (e.g., contributions from passive dynamics that are present even before learning begins).

Quantitative metrics. To characterize the motion dependence of the average single-trial responses to the FPs, we regressed the population-averaged adaptive response onto the population-averaged longitudinal position and velocity traces in the EC movements, along with an offset (Fig. 2, *D* and *H*). This regression allows us to find the position and velocity gains (k and b, respectively) modifying the position, $P(t)$, and velocity, $V(t)$, traces to find the force estimate, $\hat{F}(t)$, that most closely matches the adaptive response in a least-squares sense. This regression can be summarized in the following equation:

$$\hat{F}(t) = k \cdot P(t) + b \cdot V(t) + \text{offset} \quad (6)$$

To compare the shapes of the single-trial adaptive responses to the FPs and FFs in the time domain, we normalized the population-averaged responses by the peak force value (Fig. 3, *C* and *G*). This allows us to identify how similar or different these adaptive responses are to each other, potentially providing insight into how the motor system adapts to the FPs. To compare the single-trial adaptive responses to the FPs and FFs in gain-space, we regressed the subject-averaged responses onto the subject-averaged position and velocity traces in the direction of motion (i.e., the longitudinal traces), along with an offset, and plotted the standard error ellipses representing the position and velocity gains in normalized gain-space (Fig. 3, *D* and *H*). To characterize the motion dependence of the asymptotic adaptive response to a 5-cm FP, we regressed the average adaptive response over the last third of training (total *trials 257–392*) onto the average longitudinal position, velocity, and acceleration traces (Fig. 4*B*).

To quantify the specificity of learning with respect to the goal, we calculated the angle in gain-space between the gain-space representations of the adaptive responses (Fig. 4*D*) and the gain-space goal (Fig. 4*E*). This metric is a one-dimensional (1D) measure that can quantify the alignment of the motor output with the projection of the learning goal into gain-space, and it allows us to characterize the changes in the shape of the adaptive responses [i.e., we can see the relative changes of the 3 kinematic variables in 3-dimensional (3D) position/velocity/acceleration space]. To quantify the size of the component of the adaptive response that is aligned with the FF goal in the extended-exposure paradigm (*experiment 3*), we projected the data in gain-space onto the gain-space goal and then normalized by the goal length to obtain an adaptation index between 0 and 1, with 0 corresponding to no learning and 1 corresponding to full learning [Fig. 4*F*, analyzing only position and velocity (blue trace) and analyzing position, velocity, and acceleration (black trace)]. The gain-space analysis throughout this report is performed to help provide intuition about the relative contributions of position, velocity, and acceleration to the learning process. We also regressed the adaptive responses onto the 5-cm FP trace to quantify the amount of adaptation along the dimension of the FP shape (Fig. 4*F*, magenta trace).

Alternative basis functions. We used the longitudinal position, velocity, acceleration, jerk (3rd derivative of position), and snap (4th derivative of position) traces measured during EC probe trials as basis functions for the adaptive response to extended exposure to the 5-cm FP. To provide a comparison to other reasonable basis sets, we also analyzed how well the data were fit by *1*) the lateral position, velocity, and acceleration traces measured during pulsed trials and *2*) a smooth but non-motion-dependent polynomial basis set with up to 20 parameters/orders. For example, a 4th-order polynomial would take the form $y(t) = k_0 + k_1x(t) + k_2x(t)^2 + k_3x(t)^3 + k_4x(t)^4$.

Analysis of trial-to-trial fluctuations in the adaptive response. This analysis examined whether trial-to-trial fluctuations in the adaptive responses can be explained by changes in movement speed and acceleration from one trial to the next. We identified the slowest and fastest 33% of movements for each subject, based on peak y-velocity, in the asymptotic learning period of extended training (*trials 257–392*). We then bootstrapped these two data sets, using 20,000 iterations with replacement to find the bootstrapped average force pattern associated with each speed grouping (Fig. 6, *C* and *D*). To characterize the motion dependence for the slow movement data, we regressed each one of the 20,000 bootstrapped force patterns onto the corresponding position, velocity, and acceleration patterns, all obtained from the slow movement data. To evaluate whether this motion dependence in the slow data can predict the motor output in the fast data, we generated three models for the fast data based on the slow data. The raw time-based model is the exact copy of the best-fit

Downloaded from http://jn.physiology.org/ at Harvard Univ on July 1, 2013

position/velocity/acceleration (PVA) fit for the slow data (Fig. 6*D*), the temporally scaled time-based model is a compressed form of the raw time-based model (Supplemental Fig. S3*A*), where the compression ratio is the ratio required for the slow velocity profile (Fig. 6*A*) to be above 0.05 m/s for the same amount of time as the fast velocity profile (Fig. 6*A*), and the motion-based model is derived from application of the coefficients of the PVA fit for the slow data onto the motion profiles for the fast movement data for each one of the 20,000 bootstrap iterations (Fig. 6*D*). For the fast-to-slow predictions, the raw time-based model is the exact copy of the best-fit PVA fit for the fast data (Supplemental Fig. S3*B*), the temporally scaled time-based model is a stretched form of the raw time-based model (Supplemental Fig. S3*B*), where the stretching ratio is the ratio required for the fast velocity profile (Fig. 6*A*) to be above 0.05 m/s for the same amount of time as the slow velocity profile (Fig. 6*A*, slow trace), and the motion-based model is derived from application of the coefficients of the PVA fit for the fast data onto the motion profiles for the slow data (Supplemental Fig. S3*B*). We recorded the R^2 values for each one of these fits and averaged them together to find the mean and standard deviations, which we display in Fig. 6*E*. Note that the R^2 values for the best-fit data do not have error bars because we performed these motion-dependent regressions on the average force and motion profiles. For the combined analysis of the slow-to-fast and fast-to-slow predictions, we sum the residuals of the model fits and the variances of the data sets for both predictions to calculate the combined R^2 values.

Comparison of single-trial learning and extended results. To compare the single-trial learning and first and last bins of extended learning, we looked at five different metrics: *1*) the force adaptation at the time of the FP peak (Fig. 7*A*), *2*) the R^2 for a PVA motion-based regression for the adaptive responses (Fig. 7*B*), *3*) the R^2 for a FP-based regression (Fig. 7*C*), *4*) the partial R^2 for acceleration on top of a PV fit (Fig. 7*D*), and *5*) the partial R^2 for the FP on top of a PVA fit (Fig. 7*E*). The first metric was calculated from the raw data, while the remaining four metrics were calculated from data sets generated by a bootstrapping routine (1,000 iterations, with replacement).

Correlations between previously studied force perturbations and motion-state. Two previous studies have looked at the adaptation to somewhat complex perturbations for which the extent of the linear motion dependence was somewhat unclear. In these studies, the perturbations were either nonlinearly dependent on motion or dependent on time. To discuss these studies thoroughly (see *Previous work on non-motion-dependent learning*), we thought that it was worthwhile to characterize the extent to which these perturbations were linearly motion dependent by estimating the correlation coefficients between each perturbation and position, velocity, and acceleration. To estimate the motion dependence of the time-dependent force perturbation (a modified cosine function) used by Conditt and Mussa-Ivaldi (1999), we correlated the time-dependent cosine function they used with minimum-jerk motion profiles that are characteristic of point-to-point reaching arm movements. Numerically, we sampled both the perturbation profile and the motion profiles at 1,000 points in time, equally spaced, and found the correlation coefficients between the modified cosine function and the 1,000-element vectors. We used minimum-jerk motion profiles as an estimate of the motion profiles that their subjects displayed because we did not have access to the original motion data. Similarly, to find the motion dependence of the five different position-dependent force perturbations studied by Wei et al. (2010), we correlated these perturbations with minimum-jerk position, velocity, and acceleration profiles. Since these five perturbations were described and implemented as functions of position, we converted the temporal profiles of minimum-jerk movements into functions of position by interpolating the velocity and acceleration profiles onto the position profile (note that the position profile as a function of position is simply linear). These position-dependent functions of reach motion were then correlated with the position-dependent perturbations used in this study. Note that we report only the largest correlations in DISCUSSION.

RESULTS

Single-trial adaptation to force pulse perturbations reveals motion-dependent learning. A host of previous studies, including our own work, have shown that the responses to motion-dependent perturbations or perturbations that are nearly motion dependent result in motion-dependent adaptive responses (Conditt et al. 1997; Conditt and Mussa-Ivaldi 1999; Hwang et al. 2003; Sing et al. 2009). Here we studied impulse perturbations to determine whether perturbations that do not resemble position, velocity, acceleration, or combinations of them would also elicit primarily motion-dependent adaptive responses. We instructed subjects to make 10-cm reaching arm movements while grasping the handle of a robotic manipulandum (Fig. 1*A*). After a baseline familiarization period, we applied FPs through the manipulandum to subjects' hands. Note that these 18-N, 80-ms FPs approximate impulse functions, which are commonly used in system identification to characterize the behavior of a system with memory (Bellman and Åström 1970; Friston et al. 1998; Juang 1994; Koop et al. 1996). The FPs began at either 2 cm or 5 cm into the movement and generally caused lateral deviations of 3–4 cm in the hand paths (Fig. 2, *A* and *E*). We chose these two nonoverlapping impulselike force perturbations because they produced different patterns of hand path errors.

We found that the single-trial adaptive responses observed on the trials following the FPs did not resemble the shape of the narrow force perturbations that we applied (2-cm FP: $R^2 = 0.17$ for the FP fit, 5-cm FP: $R^2 = 0.10$; note that both R^2 values would have been identically 0 for infinitely narrow FPs), as shown in Fig. 2, *C* and *G*. Instead, we found that the shapes of the single-trial adaptive responses we observed were remarkably well-characterized by a positive linear combination of the position and velocity (PV) associated with the adapted movement, as shown in Fig. 2, *D* and *H* (2-cm FP: $R^2 = 0.87$ for the PV fit; 5-cm FP: $R^2 = 0.93$). Adding the acceleration trace to the motion-state basis set improves the R^2 for the 2-cm FP slightly to 0.90 but does not change the R^2 for the 5-cm FP. These findings suggest that motion-dependent motor primitives lead to an intrinsically motion-dependent coordinate system for the generation of adaptive response so that the adaptive responses to arbitrary dynamical perturbations are obligated to depend on motion for initial learning. Note that these single-trial responses can be explained by positive, linear combinations of position and velocity for both the 2-cm and 5-cm FPs, consistent with the idea that the motor primitives underlying adaptation are tuned to position and velocity in a positively correlated manner (Sing et al. 2009). Thus we hypothesized that the motor system is not adapting to the FPs themselves, but instead to motion-dependent representations of these FPs, such as their projections into the space of position and velocity (Fig. 1, *C* and *E*, see MATERIALS AND METHODS). In line with our previous findings (Sing et al. 2009), the adaptive responses to different perturbations were more similar than the perturbations themselves or the hand path errors resulting from the perturbations ($R^2 = 0.81$ for the adaptive responses to the 2-cm vs. 5-cm FPs, $R^2 = 0.64$ for the corresponding hand paths, and $R^2 = 0.001$ for the FPs themselves).

Downloaded from http://jn.physiology.org/ at Harvard Univ on July 1, 2013

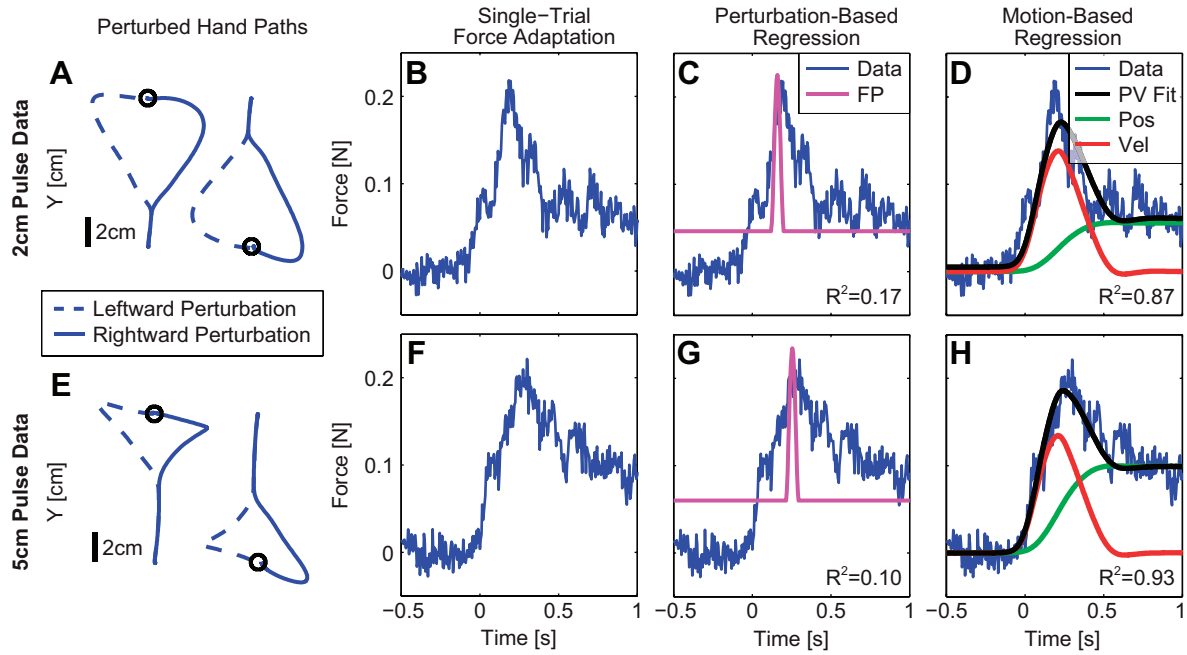


Fig. 2. Single-trial adaptation to force-impulse perturbations. Data correspond to the 2-cm (*A–D*) and 5-cm (*E–H*) FPs from *experiment 1*. *A* and *E*: perturbed hand paths caused by the FPs. Dotted lines indicate hand paths resulting from leftward-directed FPs. *B* and *F*: single-trial force adaptation to the FPs. The force patterns displayed are the difference between the post-FP and pre-FP error-clamp (EC) probe trials (see MATERIALS AND METHODS). *C* and *G*: perturbation-based regressions. The FP shape is represented by the magenta curve. R^2 values of these poor fits are at *bottom right*. *D* and *H*: motion-based regressions. The overall motion-dependent fit is shown in black, the position contribution is in green, and the velocity contribution is in red. R^2 values of these fits are at *bottom right*. All data shown are subject-averaged data.

It is important to note here that motion-dependent representations (see MATERIALS AND METHODS) cannot approximate these FPs very well (2-cm FP: $R^2 = 0.16$; 5-cm FP: $R^2 = 0.18$). The poor quality of the motion-state representation for both the 2-cm and 5-cm FPs, illustrated in Fig. 1, *B* and *D*, is evidenced by the poor match between the shapes of the FPs and the shapes of their motion-state representations. Although these representations have transient peaks in the middle of the movement (due to the velocity component), the peaks are much smaller and wider than the FP profiles, leading to the very low R^2 values.

Similar single-trial adaptation to force-pulse perturbations and motion-dependent approximations of them. If the motor system is truly adapting to the motion-dependent representations of the FPs, then we would predict that single-trial adaptive responses to such representations (Fig. 1, *C* and *E*) would be very similar to the adaptive responses elicited by the FPs themselves. Therefore, we conducted a second experiment to study how subjects adapt to motion-dependent approximations of the 2-cm and 5-cm FPs that were administered in the first experiment (Fig. 1, *C* and *E*). We obtained these approximations by projecting the FPs used in *experiment 1* into the space of position and velocity (see MATERIALS AND METHODS). A key point is that these "equivalent" FFs (so named because force is a function of the field of possible motions) can only provide a relatively poor approximation of the FP perturbations studied in *experiment 1*. Correspondingly, these equivalent viscoelastic FFs introduce lateral deviations in the subjects' hand paths (Fig. 3, *A* and *E*) that begin earlier and are significantly smaller in magnitude than those introduced by the FPs (max lateral deviations for 2-cm FP and FF: 3.8 ± 0.8 cm vs. 2.2 ± 0.5 cm, respectively, $P < 1.0 \times 10^{-12}$; max lateral deviations for 5-cm FP and FF: 3.7 ± 0.8 cm vs. 2.3 ± 0.5 cm, respectively, $P < 1.0 \times 10^{-12}$; mean ± SD). In contrast, we found that the single-trial adaptive responses to the FFs are significantly larger in magnitude than the responses to the FPs (peak forces for 2-cm FP and FF: 0.22 ± 0.0 N vs. 0.38 ± 0.14 N, $P = 9.2 \times 10^{-4}$; peak forces for 5-cm FP and FF: 0.22 ± 0.09 N vs. 0.36 ± 0.18 N, $P = 0.010$; mean ± SD). This increase in the amplitude of the adaptive response may be because the motor system adapts less to errors that it estimates as less likely to occur in the future, and the abruptness of the FPs may put them in this category (Wei and Kording 2009).

Interestingly, however, we find that the shapes of the responses to the FP and FF perturbations are extremely similar, as illustrated in the normalized traces shown in Fig. 3, *C* and *G* (2-cm FP vs. FF responses: correlation coefficient = 0.95; 5-cm FP vs. FF responses: correlation coefficient = 0.88). This suggests that, in terms of its adaptive response, the motor system effectively sees the FP perturbations as similar in shape to the motion-dependent approximations of them. Furthermore, as with the single-trial adaptive responses to the FPs, the adaptive responses to the equivalent FFs are extremely well characterized by a combination of motion-state variables (2-cm FF: PV fit $R^2 = 0.89$, PVA fit $R^2 = 0.93$; 5-cm FF: PV fit $R^2 = 0.89$; PVA fit $R^2 = 0.94$). Note that the R^2 values for the FP fits are quite close to the R^2 values for the corresponding FF fits, with all R^2 values >0.86, indicating a consistently high level of motion dependence in the motor system's response to the FPs and the equivalent FFs we studied. Since the potentially high-dimensional adaptive response shapes that we observe in the single-trial learning experiments are so well characterized by a simple, low-dimensional regression analysis, we can represent the responses in a two-dimensional (2D)

Downloaded from http://jn.physiology.org/ at Harvard Univ on July 1, 2013

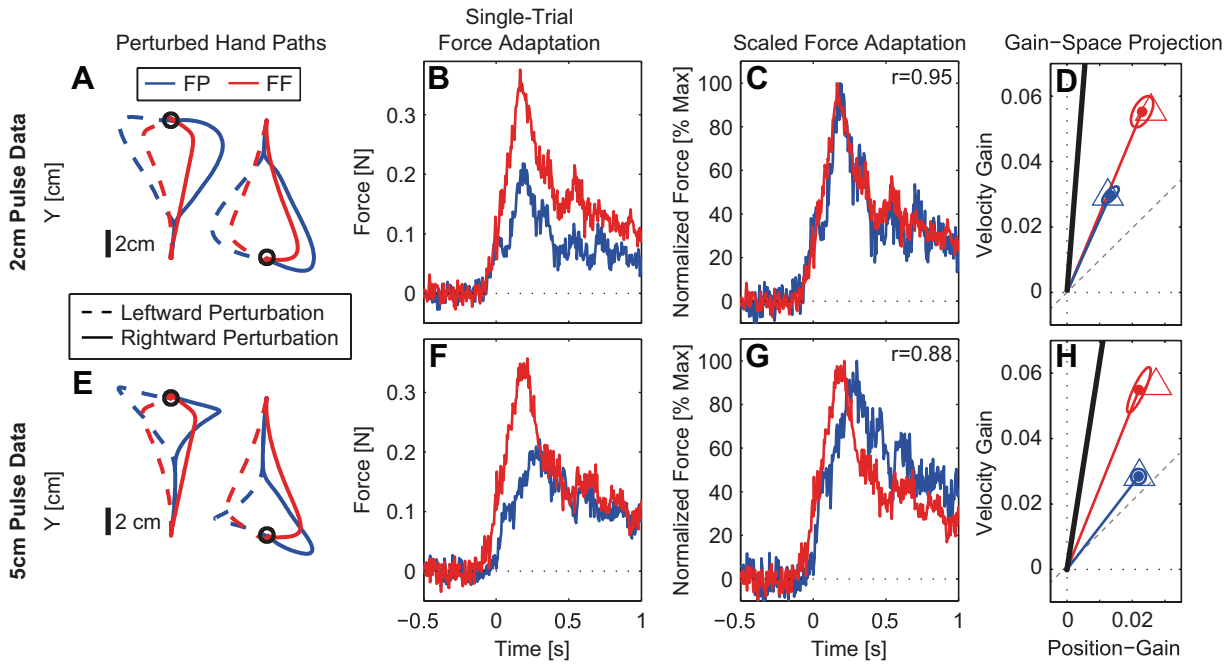


Fig. 3. Single-trial adaptation to force-impulses and motion-dependent approximations of them. Data displayed here come from *experiment 1* (FP data) and *experiment 2* (motion-dependent FF data). Data are for the 2-cm (*A–D*) and 5-cm (*E–H*) FPs (blue) and the approximating FFs (red). *A* and *E*: perturbed hand paths caused by the FPs and "equivalent" FFs. Dashed lines indicate hand paths resulting from leftward-directed FPs and FFs. Hand paths are subject-averaged. *B* and *F*: single-trial force adaptation to the FPs and FFs. The force patterns displayed are the difference between the postperturbation and preperturbation EC probe trials (see MATERIALS AND METHODS). Force patterns are subject-averaged. *C* and *G*: force adaptations normalized by the maximum force. Correlations between these shapes are at *top right*. *D* and *H*: gain-space representation of the single-trial force adaptations depicted in *B* and *F*, respectively. Black lines indicate the directions of the gain-space representations of the perturbations, as shown in Fig. 1, *C* and *E*. Ellipses represent 1 SE. Triangles indicate the gain-space representations of the mean force profiles as opposed to the mean of the gain-space representations. Diagonal dashed lines show $y = x$.

position/velocity gain-space without losing much information (Fig. 3, *D* and *H*). In this gain-space, the *x*- and *y*-coordinates are the normalized gains modifying the movement position and velocity traces, respectively, for *Eq. 6* (see MATERIALS AND METHODS). The similarity between the shapes of the adaptive responses that we observed in Fig. 3, *C* and *G*, is also reflected in the gain-space representations shown in Fig. 3, *D* and *H*. Note that the gain-space representations of all the responses we studied lie in the first quadrant, indicating that they are characterized by a positive combination of position- and velocity-dependent components. Furthermore, they are closely aligned with one another within the first quadrant [2-cm FP and FF: 69.3 ± 16.1° vs. 67.7 ± 9.2° (mean ± SD); 5-cm FP and FF: 52.4 ± 15.7° vs. 66.3 ± 12.0°]. However, the responses are not perfectly aligned with the learning goal (predominantly a velocity-dependent perturbation, see Fig. 1, *C* and *E*) but are instead rotated toward the center of the first quadrant of the PV gain-space. This observation is in line with our previous results (Sing et al. 2009), which show that such rotation occurs because the majority of primitives with positive velocity responses also have positive position responses due to the motor primitives that display positively correlated dependence on the position and velocity of limb motion. Thus the rotated adaptive responses seen in Fig. 3, *D* and *H*, closely resemble the rotated single-trial adaptation to purely velocity-dependent FFs reported previously (Sing et al. 2009).

These first two experiments demonstrate that single-trial adaptive responses to FPs are extremely well described by a simple linear combination of motion signals ($R^2 > 0.86$ for both FPs) and that these adaptive responses are very similar in shape to the single-trial responses observed for the viscoelastic projections of these FPs into position-velocity space (correlation coefficient > 0.87 for both FP-FF pairs), even though these projections are not similarly shaped to the FPs themselves ($R^2 < 0.19$ for both FPs studied) of the trajectory errors caused by them. These findings indicate that single-trial adaptive responses are dictated by motion-dependent motor primitives.

Motion-dependent adaptation persists after extended exposure to force pulses. Do adaptive responses lose their motion dependence in order to become specifically tuned to the FPs with prolonged exposure? To answer this question, we conducted a third experiment to determine whether extended exposure to FPs increased the specificity of the adaptive response by exposing subjects to a prolonged block of trials during which the same FP was repeatedly administered. Specifically, after a baseline period of 300 trials, subjects were exposed to a block of 392 trials consisting of 300 5-cm FP trials to drive adaptation with 92 EC probe trials interspersed to measure how adaptation progressed. In this experiment, four subjects experienced leftward-directed 5-cm FPs and another four experienced rightward-directed 5-cm FPs. Figure 4*A* displays the evolution of the adaptive responses we observed during training. Inspection of these curves reveals that even after 300 trials of FP exposure, the shape of the adaptive response to the FP perturbation still does not resemble the FP perturbation itself ($R^2 = 0.14$). Correspondingly, the red trace in Fig. 4*A* (denoting the average response during *trials 368–392* of the training block) is still much wider than the narrow FP and still

Downloaded from http://jn.physiology.org/ at Harvard Univ on July 1, 2013

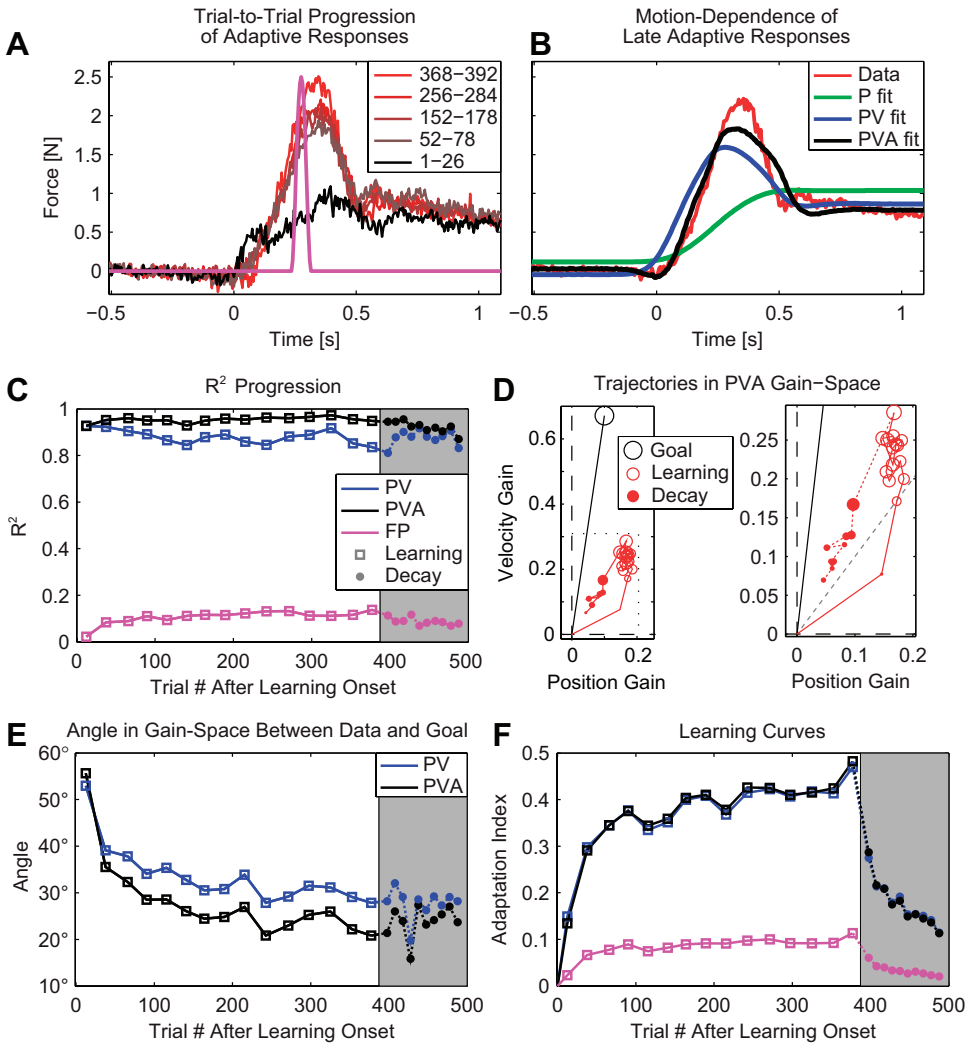


Fig. 4. Adaptation to extended exposure of the 5-cm FP. *A*: evolution of adaptive responses during extended exposure to the FP. The FP shape is represented by the magenta curve. The force patterns depicted are averaged across subjects and within bins (indicated in key). The colors of the force patterns indicate the stage of training—black is earlier, and red is later. Note that the trial numbers denoted in the key span both FP trials (300 trials) and randomly interspersed EC measurement trials (92 trials). *B*: motion-dependent representation of the average adaptive force response (red curve) over last third of training. Green curve is a fit based solely on the position trace (P), blue curve adds the velocity trace (PV), and black curve adds the acceleration trace (PVA). *C*: progression of R^2 values for PV (blue), PVA (black), and FP-based (magenta) representations of the adaptive responses. Gray region indicates the decay period in the experiment, where subjects were given 100 consecutive EC trials. Decay data are shown as dots. *D*, *left*: gain-space representation of the progression of adaptive responses. Acceleration gains are indicated by the size of the dots—larger size means greater magnitude. Filled dots indicate the decay portion of the experiment. The black outlined dot is the gain-space representation of the perturbation and is the same as in Fig. 1*E*. *Right*: zoomed-in version of representation on *left*. *E*: angles in the PV (blue) and the PVA (black) gain-spaces between the data and the learning goal. *F*: adaptation indexes representing the size of the components aligned with the PV goal (blue), the PVA goal (black), and the FP shape (magenta). All data shown are subject-averaged.

contains the static offset at the end of the movement, which is indicative of the position-dependent learning we observed in our single-trial learning data (Fig. 2*H*).

If the FP shape cannot explain the adaptive responses, then how does a motion-dependent representation fare? Since there is very little change in the adaptive responses over the last third of training (*trials 256–392*), we averaged these responses together to obtain a robust estimate of the asymptotic adaptive response after prolonged exposure to the 5-cm FP perturbation. Surprisingly, we found that this asymptotic response was extremely well characterized by a motion-dependent representation, as shown in Fig. 4*B* (position fit, $R^2 = 0.47$; PV fit, $R^2 = 0.85$; PVA fit, $R^2 = 0.95$). This indicates that the motion dependence in early learning resulting from the motion dependence of the motor primitives does not disappear with extended training. Instead, it continues to dominate the adaptive response even after 300 trials of FP exposure.

Evolution of motion-dependent adaptive responses during extended training. Remarkably, we find that the ability of a motion-dependent representation to characterize the adaptive responses is maintained throughout all 15 blocks of the extended training period (Fig. 4*C*). The R^2 values characterizing the goodness of fit are consistently above 83% for the PV analysis and above 92% for the PVA analysis. These consistently high R^2 values underscore the degree to which motion-dependent motor primitives underlie the adaptive responses, not only in single-trial learning but also throughout the extended learning block. However, despite the consistency with which motion-dependent representations explain the adaptive response, the composition of these representations evolves during training (i.e., the relative contributions of position, velocity, and acceleration change).

Consistent with our single-trial learning results for the 5-cm FP, acceleration makes essentially no contribution to the adaptive response in the first block of training. However, as training proceeds the acceleration contribution becomes more prominent—this can be visualized by the increasing separation between the R^2 values of PV and PVA fits illustrated in Fig. 4*C*. Correspondingly, the partial R^2 for acceleration on top of position and velocity begins at 0.01 for the first bin and increases to 0.39 and then 0.58 in the second and third bins, respectively, eventually reaching 0.68 by the end of training for the subject-averaged force profile data. We find that the goodness of fit for the FP representation of the adaptive responses also improves during the extended training period, indicating that the adaptive responses are becoming more FP-like, as shown in Fig. 4*C*. Despite this improvement, the goodness of fit for the FP representation never exceeds an R^2 value of 14%

Downloaded from http://jn.physiology.org/ at Harvard Univ on July 1, 2013

and is dwarfed by the ability of the motion-dependent representation to explain the data ($R^2 > 83\%$). Although the goodness of fit for the FP perturbation does improve during training (from $R^2 = 0.02$ in the 1st block to 0.14 in the 15th block; $P = 0.01$, paired t-test across R^2 values for individual subjects), this improvement appears to asymptote by the 4th or 5th block—about a third of the way into the extended training period and at approximately the same time as the difference between the PV and PVA R^2 curve asymptotes (Fig. 4*C*).

This observation raises the question of whether the growth of the acceleration contribution explains the improved FP goodness of fit or the improved FP goodness of fit somehow explains the apparent growth of the acceleration contribution. To investigate, we directly compared the ability of the acceleration trace and the FP trace to explain the shape of the adaptive response beyond its viscoelastic component in the last bin of learning. We found that the partial R^2 for the acceleration trace on top of the PV fit (0.68) was far greater than the corresponding partial R^2 (0.04) for the FP trace ($P = 0.002$, paired t-test across partial R^2 values for individual subjects). Similarly, we found that the partial R^2 for the acceleration trace on top of a PV+FP fit (0.67) was far greater than the corresponding partial R^2 (0.006) for the FP trace on top of a PV+A fit ($P = 0.002$, paired t-test across partial R^2 values for individual subjects). This analysis demonstrates that the improved goodness of fit of the FP representation occurs within the PVA space, and that very little adaptation is occurring outside of this space.

How does the emergence of the acceleration component in the adaptive response lead to an improvement in FP specificity? Comparison of the PV and PVA fits for the asymptotic adaptive response shown in Fig. 4*B* provides some insight. The transient portion of the PVA fit for asymptotic learning is sharper and slightly delayed compared with the transient portion of the asymptotic PV fit. These changes are due to *1*) a negative trough in the acceleration contribution early in the movement, which delays the rise of the adaptive response compared with the PV fit, and *2*) a positive peak in the acceleration component late in the movement, which increases the late portion of the motion-dependent adaptive response, delaying the peak and further sharpening it compared with the PV fit. The sharpening of the motion-dependent adaptive response afforded by the emergence of the negative acceleration component allows this response to resemble the shape of the FP more closely, which starts at the midmovement point, peaks around 6 cm, and terminates around 7 cm. However, it is important to note that the improved specificity resulting from the acceleration component is limited, as the R^2 value for the alignment of the adaptive response with the FP never rises above 14%.

Further analysis of the evolution of the motion-dependent representations reveals that these representations grow closer to the equivalent FF as training proceeds. This growth can be seen clearly in 3D PVA gain-space in Fig. 4*D*, where the equivalent FF (i.e., the gain-space representation of the FP) is represented as the black dot, the open circles represent the adaptive responses during learning, and the size of the dots denotes the relative size of the acceleration contribution. Initially, the learning is poorly aligned with the direction of the equivalent FF in gain-space—deviated clockwise from the predominantly velocity-dependent FF goal, similar to the behavior we previously observed for purely velocity-dependent FF learning (Sing et al. 2009). However, with training, the magnitude of the responses increases, while the alignment improves. Although the position contribution remains relatively constant, the magnitudes of both the velocity and acceleration contributions increase while drawing closer to the gain-space representation of the FP (i.e., the equivalent FF).

We quantify the "closeness" of the adaptive responses to the FF goal with two metrics: *1*) the angles in gain-space between the data and the FF goal, which represent the specificity of learning for the equivalent FF (Fig. 4*E*), and *2*) the projection of the data onto the FF goal, which represents the size of the component of the adaptive response that is aligned with the FF goal (Fig. 4*F*, see MATERIALS AND METHODS). We find that the angles steadily decrease for both the PV and PVA representations, indicating that the specificity of the adaptive response steadily increases during the course of training. Note that the angles in PVA space are smaller than the angles in PV space, showing that there is greater alignment between the adaptation and learning goal when acceleration is incorporated into the motion representation.

In addition to the increased specificity of learning, the size of the component of the adaptive response specific to the FF also increases (Fig. 4*F*). This magnitude is captured by an adaptation index, which ranges from 0 to 1, corresponding to no specific learning and complete learning, respectively (see MATERIALS AND METHODS). Both the PV and PVA learning curves exhibit rapid initial learning but then slow down and asymptote at an adaptation index of ~0.43. In comparison, adaptation along the dimension of the FP shape asymptotes at an adaptation index of ~0.10 (Fig. 4*F*), well below the level of the motion-dependent adaptation. Furthermore, the FP adaptation levels are fully explained by changes in the motion dependence of the adaptive responses, as demonstrated by the partial R^2 analysis performed above. Taken together, these findings reveal that although a motion-dependent representation is consistently maintained throughout a period of extended adaptation, the nature of this representation evolves for the 5-cm FP perturbation we studied. The adaptation starts off as almost purely viscoelastic, but a negative acceleration component emerges with prolonged training over the course of the first few blocks, which sharpens the adaptive response so that it better approximates the shape of the FP perturbation (as in Fig. 4*B*) and increases the specificity of the adaptive response (Fig. 4*E*). Although sharpening occurs, the degree to which it can take place is limited by the width of the acceleration profile, and thus at asymptote the sharpening is far less than what would be required to specifically compensate the FP perturbation. Correspondingly, we find that the onset of the adaptive response (defined as the time after movement onset when the lateral force first becomes significantly different from baseline) also shows a limited improvement in specificity during training as shown in Supplemental Fig. S2. During the first 20 trials of training, the onset of the adaptive response occurs 70 ms after the movement onset, preceding the perturbation onset by 145 ms. Then, as training proceeds, the onset of the adaptive response becomes more closely aligned with perturbation onset. The adaptive response onset gradually shifts closer to the perturbation onset such that it precedes perturbation onset by an average of 80 ms over the last two-thirds of the training period, but there is no further improvement over the last

Downloaded from http://jn.physiology.org/ at Harvard Univ on July 1, 2013

two-thirds of the perturbation period as shown in Supplemental Fig. S2. The learning curve for this shift in the onset timing of the adaptive response is consistent with a reshaping of the adaptive response during extended training that asymptotes well short of fully specific compensation of the FP perturbation.

We have demonstrated that the adaptive responses produced during extended exposure to the 5-cm FP can be well characterized by the basis set of reach position, velocity, and acceleration (high R^2 values for PVA regressions—the black trace in Fig. 4*C*). Although it is possible that this finding merely indicates that the PVA basis set is particularly flexible in that it can characterize arbitrary force patterns, the gradual reduction in the gain-space angle between the learning goal and data during extended training (Fig. 4*E*) and the data presented in Fig. 5 both suggest otherwise. This gradual reduction in gain-space angle during training reflects compositional changes within the PVA dependence that indicate more specific tuning of the adaptive response to the gain-space goal, an observation that would be expected if the PVA basis set were the appropriate basis set for motor adaptation but would not be expected for a generic basis set. In particular, a negative acceleration component emerges that helps the adaptive responses to reflect the 5-cm FP shape with increasing (although somewhat limited) fidelity. This is in contrast to the finding that the FP shape does a poor job of characterizing the adaptive responses during extended training as evidenced by the low R^2 values for FP regressions (magenta trace in Fig. 4*C*). Note, however, that even if the motor system intends to produce FP-like adaptive responses, the limits of human motor capabilities prohibit rapid changes in joint torque. Thus the non-FP-like adaptive responses we measure may be a reflection of physiological constraints. But perhaps the most interesting part of our results is that of the entire space of physiologically realizable adaptive responses, the motor system produces adaptive responses that are specifically motion dependent and, in particular, are a simple linear combination of the position, velocity, and acceleration traces associated with the movement. That is, the adaptive responses are not merely a slowed-down or low-pass-filtered approximation of the fast dynamics of the force perturbation, but rather they reflect motion-dependent learning. This finding, coupled with the observation that neurons in primary motor cortex (Ashe and Georgopoulos 1994; Paninski et al. 2004; Stark et al. 2007; Wang et al. 2007), premotor cortex (Ashe and Georgopoulos 1994), and cerebellum (Coltz et al. 1999; Fu et al. 1997; Shidara et al. 1993) often display nearly linear motion-dependent responses, suggests a strong relationship between what is represented in motor regions of the brain, what motor outputs are physiologically realizable, and what novel dynamics are learnable.

The decay of force-pulse adaptation is motion dependent. We find that the motion dependence we observe in the acquisition of the FP memory is also present during the decay of the memory. After the prolonged exposure to the 5-cm FP subjects continued to make point-to-point reaching movements, but we discontinued the FP perturbations and administered a block of 100 consecutive EC trials. These trials allowed subjects to perform movements associated with motor adaptation, but without the error feedback that fuels learning (Criscimagna-Hemminger and Shadmehr 2008; Scheidt et al. 2000; Sing et al. 2009; Sing and Smith 2010; Smith et al. 2006). Thus these EC trials allow us to measure the trial-to-trial active decay of the motor adaptation learned in the previous block of the experiment.

Not surprisingly, we found that the strength of the motor memory decreased during the decay period, consistent with previous results (Cohen et al. 2004; Fernandez-Ruiz et al. 2004; Scheidt et al. 2000; Smith et al. 2006). Specifically, in Fig. 4*D*, the adaptive responses during the decay period become closer to the origin, indicating a reduction in the levels of motion-dependent motor output. This decay leads to a reduction in the component of the adaptive response that is aligned with the equivalent FF, as shown in Fig. 4*F*.

However, we found that the motion-dependent nature of the adaptive response persists throughout the decay period. Although the amplitude of the adaptive response decreases by a factor of 3, we find that the extent to which this adaptive response is explained by motion is essentially unchanged. This is evidenced by the behavior of the R^2 values plotted in the decay period of Fig. 4*C*. Interestingly, we found that the pattern of motion dependence established during the extended training period was maintained as the adaptation decayed. By this we mean that the relative levels of position, velocity, and acceleration dependence were held constant during the decay period although the absolute values of these quantities were substantially reduced. Thus the multidimensional pattern by which the motion-dependent adaptation evolved during the training period was followed by a 1D recession during the decay period. This effect is evidenced by the constancy of the gain-space angles observed during the decay period in Fig. 4*E*. The angles displayed here are the 2D angles between response and learning goal in PV space and the 3D angles in PVA space. This effect is visualized in Fig. 4*D*, where the adaptive responses during this decay period display hysteresis by decaying directly back to the origin instead of returning along the path of adaptation. The observed decay behavior could arise if the motor primitives underlying adaptation were Markovian (i.e., if each primitive's decay effectively depended only on its current activation state rather than its history of adaptation) (Duda et al. 2004) and decayed at a rate proportional to the other primitives in the population.

Analysis of alternative basis sets reveals the efficiency of motion-state representations. We have supported our claim that the adaptive responses to the FPs are motion dependent by showing that they are remarkably well characterized by a linear combination of the position, velocity, and acceleration traces (Fig. 5*A*, same as Fig. 4*B*). However, it is possible that other reasonable basis sets might do just as well. We therefore compared the extent to which different basis sets could account for the adaptive responses we observed. The goodness of fit for linear regressions using the longitudinal motion states that we have focused on is displayed in Fig. 5*D* with reddish dots. With just three parameters (the zero, 1st, and 2nd derivatives of position, not counting the constant offset term), the longitudinal fit achieves an R^2 of 0.96. The addition of velocity and acceleration to the P and PV fits results in the reduction of the residual by 66% and 76%, respectively. However, additional terms based on jerk (the 3rd derivative of position) and snap (the 4th) lead to negligible improvements in the longitudinal state regression (R^2 improvements of <0.001 each, corresponding to a partial R^2 of $<10\%$ when adding these 2 variables together), suggesting that position, velocity, and

Downloaded from http://jn.physiology.org/ at Harvard Univ on July 1, 2013

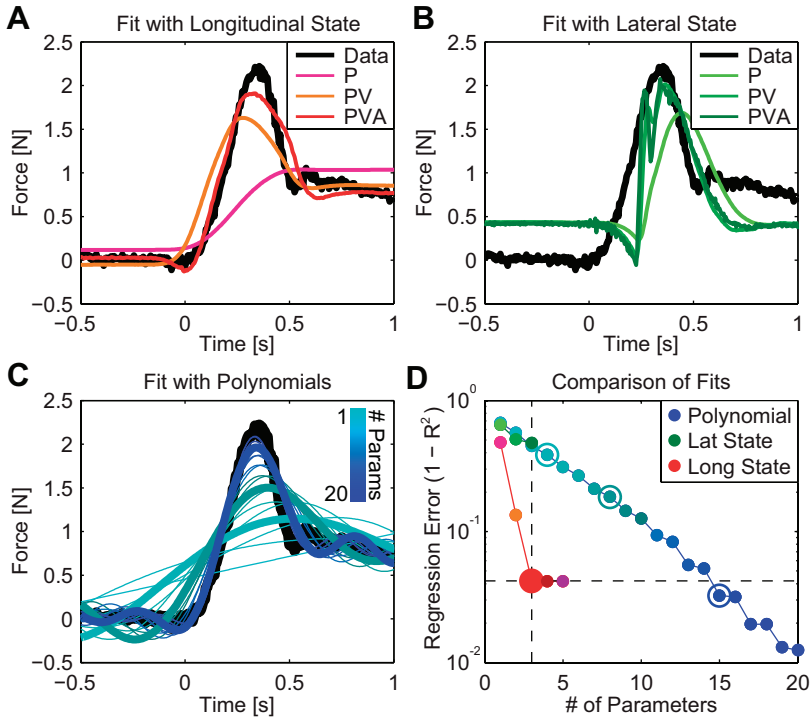


Fig. 5. Alternative basis sets. *A*: longitudinal motion-state basis set for representing the asymptotic adaptive response (*trials 257–392*; black trace). This panel is a duplicate of Fig. 4*B*. *B*: lateral state basis set for representing the asymptotic adaptive response. *C*: polynomial basis set for representing the asymptotic adaptive response. The bluer the trace, the higher the order of the polynomial (and the more parameters). Several individual fits are highlighted for the sake of clarity. These corresponding data points are highlighted in *D*, which compares the different basis sets according to their regression error as a function of the number of parameters in the model. Each fit is represented by a dot in this panel. Although only 3 fits are shown in *A*, there are 5 dots in the reddish family of longitudinal state fits. The fourth and fifth dots represent the additions of jerk and snap to the PVA regression. Dashed black lines indicate the number of parameters and the regression error associated with the 3-parameter PVA longitudinal state fit.

acceleration may be the primary states with which the motor system represents dynamics. How well do other basis sets characterize the adaptive responses to the FP?

Another possible set of basis functions is the lateral position, velocity, and acceleration. The FPs are applied in the direction lateral to movement, leading to kinematic disturbances that are almost entirely experienced in the lateral plane. The adaptive responses elicited by these lateral disturbances are also produced in this same lateral plane. Therefore, it seems reasonable that the motor system might construct or augment its adaptive responses with this particular basis set of lateral kinematic variables (Fig. 5*B*). However, a three-parameter lateral PVA fit yields an R^2 of only 0.53 (Fig. 5*D*), substantially worse than the three-parameter longitudinal PVA fit ($R^2 = 0.96$), which displays 10-fold smaller residuals. Moreover, augmenting the longitudinal PVA fit with the lateral PVA variables results in little improvement in the ability to explain the shape of the adaptive response (the total R^2 improvement is 0.008, corresponding to partial $R^2 < 22\%$ for the addition of the 3 lateral PVA variables). Why might this be the case? One possibility is that the position and velocity excursions of lateral motion are substantially smaller in magnitude than in longitudinal motion, although it should be noted that the peak lateral accelerations are much higher because of the strength of the force-impulse. A second possibility is that the lateral motion largely represents lateral errors, which may be difficult to predict. It should be noted that motion-dependent adaptive responses cannot be based on sensory feedback (visual or proprioceptive) about motion in real time because of sensorimotor loop delays (Bhushan and Shadmehr 1999; Wagner and Smith 2008). Instead, feedforward adaptive responses must be programmed in advance based on predictions about motion. Therefore, the inability to accurately predict lateral motions would likely minimize their contributions to the adaptive response.

We next investigated whether a smooth but non-motion-dependent basis set could approximate the adaptive responses as well as the longitudinal state. We used polynomial fits of increasing orders to approximate the adaptive responses as illustrated in Fig. 5*C*. Note that several individual examples are highlighted for the sake of clarity and note that as we increase the order of the polynomial basis set (i.e., the number of terms in the polynomial representation), the R^2 values improve, as expected (Fig. 5*D*), but much more slowly than fits with the longitudinal states. For example, it is not until we reach a 15th-order polynomial (and thus a 15-parameter fit) that the R^2 value for the 3-parameter longitudinal fit is surpassed. This corresponds to an average improvement of 18% per parameter for the polynomial basis set, which is similar to the 14% improvement per parameter observed for the lateral state basis set but in marked contrast to the 71% improvement per parameter observed with the longitudinal PVA fit. Note also that for the first three parameters for the polynomial fit the R^2 values are very similar to those for the lateral state fits, suggesting that the motor system relies on lateral states to no greater extent than arbitrary, non-motion-dependent polynomial representations. Although the polynomial basis set can explain the adaptive responses better than the longitudinal states, it needs fivefold more parameters to do so. Thus the longitudinal position, velocity, acceleration motion-state representation provides a substantially more efficient characterization of the adaptive response.

Trial-to-trial fluctuations in the adaptive response are explained by motion-dependent learning. Up to this point, we have shown that adaptive responses to force-impulse perturbations are remarkably well explained by simple, linear combinations of position, velocity, and acceleration traces, for both single-trial adaptation and extended learning, and that the ability of these motion traces to characterize the adaptive response persists during active decay. This suggests that the motor system forms a motion-dependent representation of the dynamic environment even when such a representation does not fit the

Downloaded from http://jn.physiology.org/ at Harvard Univ on July 1, 2013

environment particularly well, as in the case of force-impulse perturbations. Interestingly, such a representation would predict that trial-to-trial fluctuations in the velocity and acceleration of movement would lead to corresponding fluctuations in the amplitude of the feedforward adaptive response, even if no such fluctuations exist in the environment. This would occur if the position, velocity, and acceleration gains quantifying the motion dependence were stable from one trial to the next, because the larger-magnitude velocity and acceleration traces on the faster trials would result in larger adaptive responses. This insight is in line with the basic idea that the generalization of motor output across different conditions provides a window into the motor system's internal representations (Baraduc and Wolpert 2002; Bays and Wolpert 2006; Brayanov et al. 2012; Conditt et al. 1997; Conditt and Mussa-Ivaldi 1999; Ghahramani et al. 1996; Gonzalez Castro et al. 2011; Hwang et al. 2003, 2006; Joiner et al. 2011; Krakauer et al. 2000; Mattar and Ostry 2007, 2010; Morton et al. 2001; Morton and Bastian 2004; Quaia et al. 2010; Shadmehr and Mussa-Ivaldi 1994; Smith and Shadmehr 2005; Wagner and Smith 2008).

Can trial-to-trial fluctuations in the adaptive responses observed in our data be explained by trial-to-trial fluctuations in movement speed and acceleration, even though the perturbations experienced were independent of speed and acceleration? To answer this question, we focused on the asymptotic data from *experiment 3* (i.e., the last third of training, see Fig. 5) and analyzed the slowest and fastest 33% of movements for each subject, based on peak velocity (see MATERIALS AND METHODS). Note that the average peak speeds were 0.29 m/s and 0.35 m/s (a 23% difference; Fig. 6*A*) and the average peak accelerations were 1.4 m/s^2 and 2.0 m/s^2 (a 43% difference; Fig. 6*B*). We compared three simple models for explaining the shapes of these adaptive responses. A raw time-based model would predict identical adaptive responses on slow versus fast trials. A temporally scaled time-based model would predict adaptive responses that do not change in amplitude but are stretched or compressed with the movement duration for slow or fast trials, respectively. Finally, a motion-based model would predict larger adaptive responses for the fast trials. The average force patterns for these slowest and fastest movements are displayed

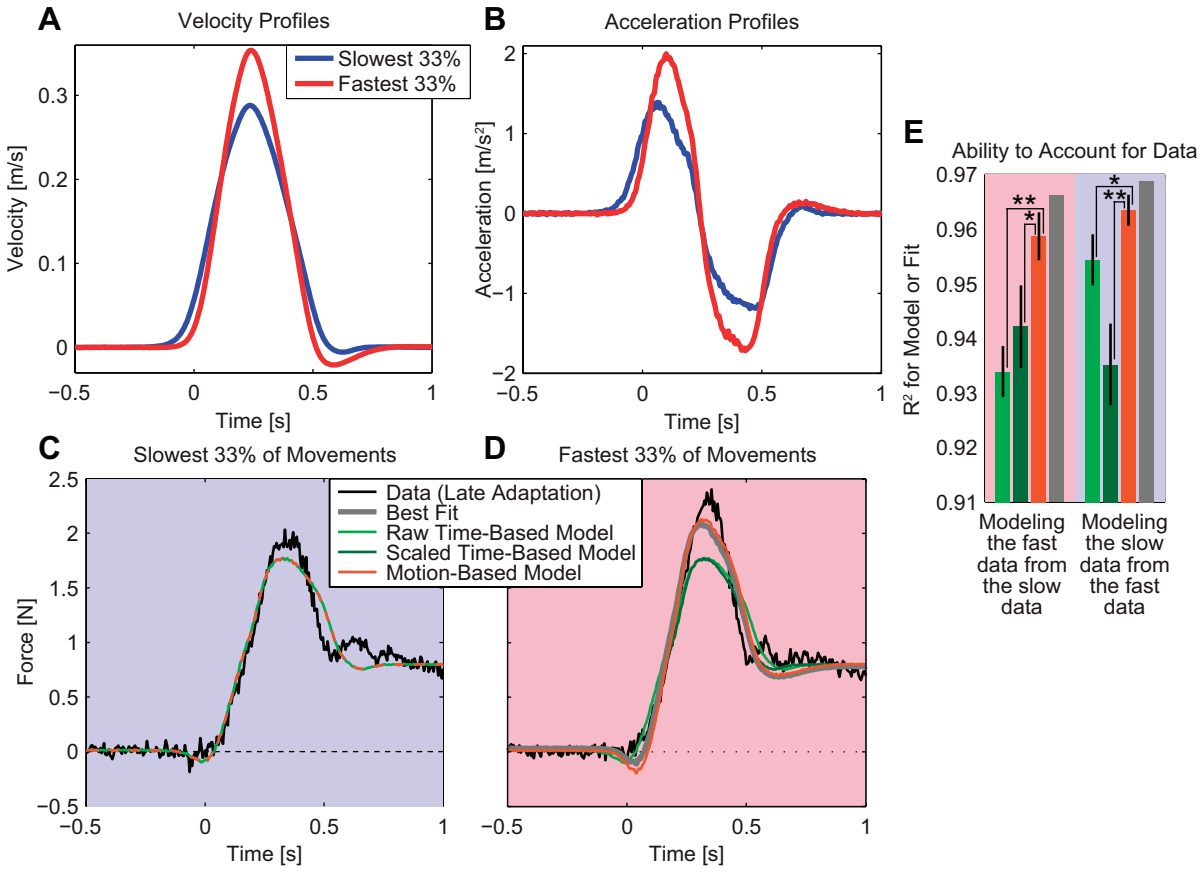


Fig. 6. Analysis of trial-to-trial fluctuations in the adaptive response. *A* and *B*: average velocity traces (*A*) and average acceleration traces (*B*) for the slowest 33% and fastest 33% of the movements for each participant. *C*: data and fits for the slowest 33% of movements during the asymptotic learning period. The average force pattern is shown in black, and the best-fit motion representation is shown as the green-orange checkered trace, to denote that this fit represents the origin of both time-based and motion-based extrapolations presented in *D*. *D*: data and fits for the fastest 33% of movements during the asymptotic learning period. Data are shown in black, the best-fit motion representation for this fast data set is shown in gray, the raw time-based model, which is identical to the best-fit trace in *C*, is light green, the temporally scaled time-based model, which is a compressed form of the raw time-based model, is dark green, and the motion-based extrapolation is orange (see MATERIALS AND METHODS). *E*: R^2 values for the models and fits. The pink background represents prediction of the fast data from the slow data as illustrated in *C* and *D*, whereas the purple background represents prediction of the slow data from the fast data. Note that the curves showing the actual predictions for this second (purple) set of R^2 values are included in Supplemental Fig. S3. Light green bars represent the ability of raw time-based models to explain the data, dark green bars represent the ability of temporally scaled time-based models to explain the data, orange bars represent the ability of the motion-based models to explain the data, and gray bars represent the best-fit motion-dependent representations. Error bars represent bootstrap SDs. $^*P < 0.05$, $^{**}P < 0.001$.

Downloaded from http://jn.physiology.org/ at Harvard Univ on July 1, 2013

as the black traces in Fig. 6, *C* and *D*. Note that the average peak forces were 2.0 N and 2.4 N for the slow and fast movements, respectively—an 18% increase for the fast movements, qualitatively consistent with the motion-based model.

To quantitatively evaluate these three models for their ability to predict the fast data from the slow data, we compared *1*) the raw time-based model: the force trace taken directly from the PVA fit of the slow movements (light green trace in Fig. 6*D*), *2*) the temporally scaled time-based model: the force trace taken from the PVA fit of the slow movements, but compressed (see MATERIALS AND METHODS), *3*) the motion-based model: the force trace derived from application of the coefficients of the PVA fit for the slow movement data onto the motion profile for the fast movement data [orange trace in Fig. 6*D*; note that both light green and orange traces in Fig. 6*D* (fast data) originate from the green-orange checkered trace in Fig. 6*C* (slow data)], and *4*) the best-fit representation: the force trace taken directly from the PVA fit of the fast movement data (gray trace, Fig. 6*D*). The raw and temporally scaled time-based models are able to explain the fast data quite well with R^2 values of 0.934 ± 0.005 (Fig. 6*E*) and 0.942 ± 0.008 (Fig. 6*E*), respectively. Remarkably, however, the motion-based model does an even better job (R^2 = 0.959 ± 0.004; Fig. 6*E*; $P < 0.001$ and $P < 0.05$ for comparisons with the raw and temporally scaled time-based models, respectively) and is very similar to the best-fit motion representation (R^2 = 0.966). The motion-based model yields reductions of 77% and 69% in the amount of variance unexplained by the raw and temporally scaled time-based models, respectively, compared with the best-fit motion representation of the fast data.

We then reversed this analysis to predict the slow data from the fast data. Again, we found that the motion-based model consistently outperformed the time-based models (R^2 = 0.954 ± 0.005 for raw time-based model, R^2 = 0.935 ± 0.008 for temporally scaled time-based model, R^2 = 0.964 ± 0.003 for motion-based model; $P < 0.05$ and $P < 0.001$, respectively). Compared with the best-fit motion representation of the slow data (R^2 = 0.969), the motion-based model yields reductions of 63% and 84% in the amount of variance unexplained by the raw and temporally scaled time-based models, respectively. The goodness of fit is illustrated for each prediction for the slow data in Fig. 6*E*, *right*. Note that the temporally scaled time-based model performs significantly worse than the raw time-based model for the fast-to-slow prediction ($P < 0.001$) and marginally better for the slow-to-fast prediction but in both cases still significantly worse than the motion-based model. Also note that the force patterns associated with the slow-to-fast predictions are illustrated in Fig. 6, *C* and *D*, and Supplemental Fig. S3*A*, and the corresponding force patterns for the fast-to-slow predictions are illustrated in Supplemental Fig. S3*B*.

If we combine the slow-to-fast and fast-to-slow predictions in terms of their ability to explain the data, the advantage of the motion-based model (R^2 = 0.961 ± 0.003) over both the raw time-based model (R^2 = 0.944 ± 0.003; $P < 0.001$) and the temporally scaled time-based model (R^2 = 0.939 ± 0.005; $P < 0.001$) is even clearer. Even though the differences between peak speeds and peak accelerations for the fast and slow movements are modest (23% and 43%, respectively), the motion-based model reduces the residual error of the raw time-based model by 31% and the residual error of the temporally scaled time-based model by 36% when combining the slow-to-fast and fast-to-slow predictions.

The ability of trial-to-trial fluctuations in movement speed to explain trial-to-trial fluctuations in the adaptive response underscores the extent to which adaptive responses are generated in a motion-dependent fashion. Small variations in movement speed invariably lead to corresponding variations in the adaptive response, even though the amplitude of the perturbing force is held constant over the entire course of the training period. This finding suggests that *1*) the same population of motion-dependent motor primitives contribute to the adaptive response in both slow and fast movements, in agreement with Joiner et al. (2011); *2*) the gains associated with these motor primitives do not systematically vary between the slowest and fastest movements in our data set; and *3*) these motor primitives have access to information about trial-to-trial fluctuations in movement velocity and acceleration (Churchland et al. 2006).

Comparison of single-trial learning and extended learning results. A quantitative comparison of the key experimental findings from our single-trial and extended learning experiments is presented in Fig. 7. This analysis illustrates how several key features of the adaptive response evolve from single-trial learning to the first block (26 trials) of the extended learning experiment to the last block of this experiment. The first feature is the amplitude of the adaptive response, which clearly increases with training as shown in Fig. 7*A* ($P < 1 \times 10^{-12}$ between single-trial learning and last bin of extended learning). The full temporal profiles associated with the growth in the adaptive response can be observed by comparing the single-trial response to the 5-cm FP displayed in Fig. 2*F* with the average responses for the first bin (*trials 1–26*) and the last bin (*trials 366–392*) of the extended learning data displayed in Fig. 4*A*. In contrast to the steady growth in the amplitude of the adaptive response, we find that the ability of a motion-dependent model to explain its shape is maintained throughout training. The R^2 values for PVA fits to the single-trial adaptive response, the first bin of learning, and the last bin of learning are 0.89, 0.87, and 0.93, respectively (Fig. 7*B*; note that these values, which were obtained by bootstrapping the data to obtain error bars, are slightly different from the previous R^2 values reported, which were calculated from the average force patterns and motion traces, see MATERIALS AND METHODS). In contrast, the perturbation-based regression does a poor job of characterizing the responses, yielding R^2 values of 0.04, 0.02, and 0.13 for single-trial learning and first and last bins of learning, respectively (Fig. 7*C*; again, these values were obtained by bootstrapping the data to obtain error bars and are thus slightly different from the R^2 values calculated from the average force patterns, see MATERIALS AND METHODS).

Although the goodness of fits for the perturbation-based regressions are poor throughout training, they do significantly improve from single-trial learning to late learning ($P < 0.01$). However, the partial R^2 for acceleration on top of a PV regression improves dramatically over this same period from 0.03 to 0.61, as displayed in Fig. 7*D* ($P < 1 \times 10^{-12}$). Is this increase in the R^2 value for the perturbation-based regression merely a consequence of the increase in the partial R^2 value for acceleration? In other words, does the increase in the specificity of the responses to the FP shape come from motion-based adaptation (and specifically its acceleration component), or does this increase in specificity come from outside the PVA space? To answer this question, we compared the R^2 values for

Downloaded from http://jn.physiology.org/ at Harvard Univ on July 1, 2013

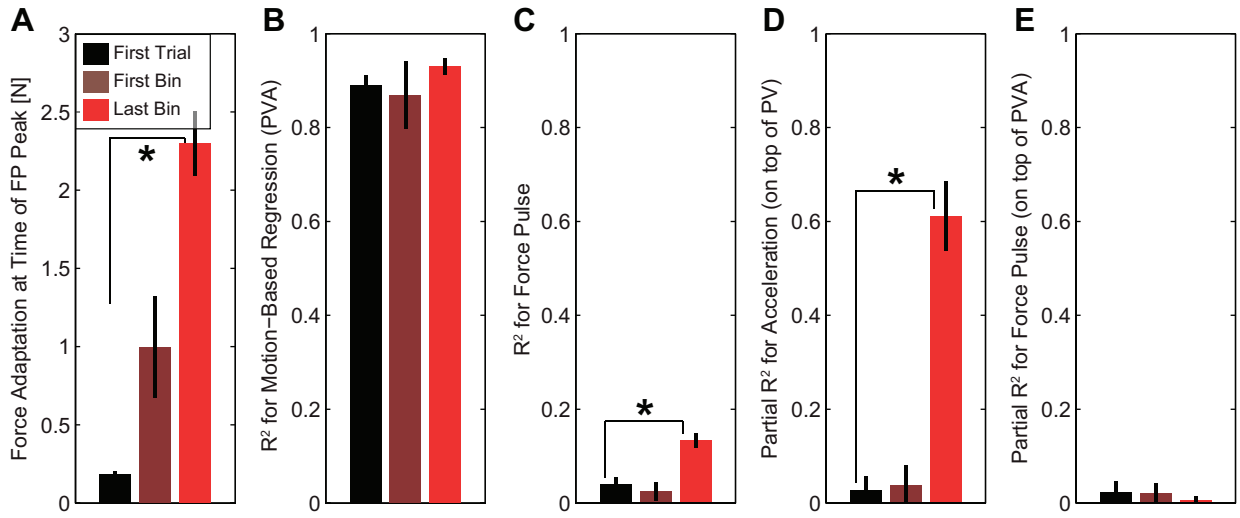


Fig. 7. Comparison of single-trial and extended learning. *A*: subject-produced force adaptation during EC trials at the time at which the peak of the FP occurs during perturbed trials. Black represents the single-trial adaptive response, brown represents the first bin (*trials 1–26*), and red represents the last bin (*trials 366–392*). Error bars are SE. *B*: R^2 values for the motion-based (PVA) regression across training. *C*: R^2 values for the perturbation-based regression across training. *D*: partial R^2 values for acceleration in the motion-based regression. *E*: partial R^2 values for the FP shape, on top of a PVA fit. Error bars for *B–E* are SDs calculated from a 1,000-iteration bootstrap. $*P < 0.01$.

the last bin of learning for fits based on *1*) position, velocity, and acceleration and *2*) position, velocity, acceleration, and the FP shape. We found these R^2 values to be extremely similar (0.9580 vs. 0.9583); correspondingly, the partial R^2 for the FP shape on top of the PVA fit was negligible (partial $R^2 = 0.005$; Fig. 7*E*). We then compared the R^2 values for fits for *1*) position, velocity, and the FP shape and *2*) position, velocity, the FP shape, and acceleration. Here, adding acceleration improved the PV+FP fit substantially (from 0.87 to 0.96), corresponding to a partial R^2 of 0.68. The fact that the addition of the FP term fails to improve the PVA fit whereas the addition of the acceleration term substantially improves the PV+FP fit suggests that the small but significant increase in the apparent FP specificity illustrated in Fig. 7*C* is mediated by the emergence of an acceleration component in the adaptation. This indicates that the tuning of the adaptive responses to the FP shape that occurs with extended training is fully explained by motion-dependent learning.

DISCUSSION

We have shown that single-trial exposure to force-impulse perturbations results in adaptive responses that are highly motion dependent in that they closely resemble a simple linear combination of the position and velocity of limb motion. Furthermore, we found that even though motion-dependent approximations of these force-impulses provide poor estimates of the shapes of these impulses and the trajectory errors caused by them, the adaptive responses to these approximations closely resemble the responses induced by the corresponding impulse perturbations. This suggests that the motor system's adaptive response to an unexpected force perturbation depends on a representation that is effectively motion dependent. Moreover, we found that prolonged exposure to a force-impulse perturbation leads to adaptive responses that grow to become not only larger but more specific to the perturbation experienced. However, this increase in specificity is mediated by the emergence of an acceleration-based component that fine-tunes the adaptive response in a motion-dependent manner rather than by reshaping it in a non-motion-dependent fashion. This fine-tuning in motion-space, which is characterized by the gradual reduction we observed in the gain-space angle between the learning goal and the observed adaptation, the decay of adaptation in a motion-dependent manner, and the ability of the motion-based model to not only explain the shapes of the average adaptive responses but also predict trial-to-trial fluctuations in these responses together provide compelling evidence that the position, velocity, and acceleration of motion form the basis set underlying motor adaptation. Correspondingly, we find that alternative basis sets constructed from a polynomial series or extended to include higher-order motion states (i.e., jerk and snap) all fail to efficiently explain the shapes of the adaptive responses. Our findings indicate that adaptive responses to arbitrary force perturbations arise from motion-dependent motor primitives based on the position, velocity, and acceleration of motion throughout the course of adaptation.

Interpreting the shapes of the observed adaptive responses: not merely smoothed versions of the environmental dynamics. The finding that the FP shape does a poor job of characterizing the adaptive responses during extended training (Fig. 4*C*) could by itself be interpreted in terms of a smoothness constraint on motor output: Even if the motor system intends to produce FP-like adaptive responses, the limits of human motor capabilities prohibit rapid changes in muscle force. Thus the non-FP-like adaptive responses we measured may be a reflection of physiological constraints on the rapidity with which force output can change. But perhaps the most interesting part of our results is that of the entire space of physiologically realizable adaptive responses, the motor system produces adaptive responses that are specifically motion dependent and, in particular, are a simple linear combination of the position, velocity, and acceleration traces associated with the movement. That is, the adaptive responses are not merely a slowed-down or low-pass-filtered approximation of the fast dynamics of the force perturbation, but rather they reflect motion-

Downloaded from http://jn.physiology.org/ at Harvard Univ on July 1, 2013

dependent learning. Indeed, smoothed versions of a force would not closely resemble the adaptive responses that we observe. Moreover, we find that this learning is refined with extended exposure to the force-impulse perturbation as evidenced by a gradual reduction in gain-space angle as shown in Fig. 4*D*. This reflects compositional changes within the adaptive response indicating a slowly increasing specificity to the gain-space goal. In particular, the gradual emergence of a negative acceleration component that helps the adaptive response reflect the force-impulse shape with increasing fidelity while maintaining a PVA R^2 value of 96% suggests that the adaptive response gradually is retuned, but within the confines of a motion-state representation.

These findings, coupled with the observation that neurons in primary motor cortex (Ashe and Georgopoulos 1994; Paninski et al. 2004; Stark et al. 2007; Wang et al. 2007), premotor cortex (Ashe and Georgopoulos 1994), and cerebellum (Coltz et al. 1999; Fu et al. 1997; Shidara et al. 1993) often display nearly linear motion-dependent responses, suggest a strong relationship between what is represented in motor regions of the brain, what motor outputs are physiologically realizable, and what novel dynamics are learnable. This correspondence, however, begs the question: Why should neural responses in motor areas and adaptive responses to environmental perturbation be linearly motion dependent? The answer to this question is not known, but one intriguing possibility is that the nature of both type of responses reflects the motor output required to compensate physical dynamics that we experience repeatedly throughout our lifetimes. Perhaps, the greatest contributors to this are the inertial dynamics of one's own limbs. Interestingly, the passive dynamics of the limb can generally be mathematically decomposed into the sum of a series of terms that each correspond to simple linear or quadratic functions of motion. Furthermore, fully linear approximations of these dynamics are often good enough that they are widely used in the control of robotic limbs (Craig 1988), suggesting that the motion-dependent learning that we observe and motion-dependent neural responses both arise from a modular solution for controlling limb dynamics employed by the motor system (Gonzalez-Castro et al. 2011; Mussa-Ivaldi and Bizzi 2000; Thoroughman and Shadmehr 2000). Further work will be required to determine whether this is indeed the case.

Previous work on non-motion-dependent perturbations. Several previous studies have looked at adaptation to non-motion-dependent force perturbations. Conditt and Mussa-Ivaldi (1999) showed that a sinusoidally shaped time-dependent force perturbation generalized in a motion-dependent fashion. However, this force perturbation was based on a modified cosine function synchronized to the requested movement duration, which closely resembles the bell-shaped velocity profile characteristic of the point-to-point movements studied ($r = 0.998$). We would argue that this time-dependent perturbation thus resembles a velocity-dependent perturbation so closely that it would readily be interpreted as motion dependent, even if the motor system does not generally interpret non-motion-dependent perturbations in this way.

Several studies have since looked at single-trial adaptation to arbitrary force perturbations that do not closely resemble simple linear combinations of motion traces (Fine and Thoroughman 2006; Karniel and Mussa-Ivaldi 2003; Wei et al. 2010). Karniel and Mussa-Ivaldi (2003) studied a sinusoidally shaped, time-varying FF that was continuously applied throughout the entire training block asynchronous with movement onset and found that subjects were unable to adapt it to it, producing no consistent aftereffects. However, because this FF was asynchronous to movement onset and the training block was several minutes in duration, successful adaptation would have required tracking the perturbation with a long-running clock that spanned the entire block of trials to allow environmental compensation to be out of phase with movement and thus independent of the motor output associated with movement. Consequently, the lack of adaptation to this FF, although suggestive of obligatorily motion-dependent adaption, may have instead reflected a limitation on the ability to generate an internal timing signal that was accurate enough to be helpful, especially since it is well known that internally generated timing signals become inaccurate at long intervals.

In line with this idea, two subsequent studies demonstrated motor adaptation when they examined non-motion-dependent perturbations that were synchronized with some aspect of the movement (Fine and Thoroughman 2006; Wei et al. 2010). These studies failed, however, to examine whether the motor adaptation was motion dependent. Fine and Thoroughman studied force-impulse perturbations very similar to the ones in our present study but initiated them at six possible locations during 10-cm reaching movements (every cm between 2 and 7 cm) rather than the two locations we examined here. They found that FPs applied at these different positions induced very similar motion aftereffects in the next movement, even though the kinematic trajectories of the pulsed movements varied widely depending on the FP onset location. This is consistent with the present findings; however, the authors made no comment about the origin of the shape they observed in the motion aftereffects. This was likely because the motions observed on aftereffect trials depend on both feedforward force patterns and feedback adaptive responses that "contaminate" the feedforward contributions (Bhushan and Shadmehr 1999). Thus they could not determine whether the aftereffect shapes reflected motion-dependent learning. The key technical feature of the present work was the ability to directly measure the temporal structure of the feedforward adaptive force responses elicited by force perturbations. We accomplish this via the use of error-clamp trials in which subjects are forced to move in a straight path to the target so that lateral errors, which drive feedback responses, are essentially eliminated, allowing the lateral component of the adaptive response to be directly measured. These measurements allow us to examine the fine temporal structure of the adaptive response to force-impulse perturbations and show *1*) that the adaptive responses to the 2-cm and 5-cm FPs are quite similar to each other ($r = 0.90$ between the two adaptive responses; Fig. 2, *B* and *F*) and *2*) that these responses are almost entirely motion dependent.

Wei et al. (2010) looked at responses to various force perturbation patterns during point-to-point reaching movements implemented as different functions of longitudinal position. Although they characterized the perturbations as "random," four of the five different force perturbations they studied closely resembled, or exactly matched, linear functions of motion-state ($r > 0.85$ between the shapes of these perturbations and either the position, velocity, or acceleration profiles of a minimum-jerk movement). Their "double-sine" perturbation, however, did not resemble the minimum-jerk profile for position, velocity, or acceleration ($r < 0.39$) and could thus be

Downloaded from http://jn.physiology.org/ at Harvard Univ on July 1, 2013

considered not motion dependent. The authors reported that the initial adaptive response to this perturbation was similar in shape to the other four perturbations they examined and thus concluded that initial adaptation was nonspecific. However, as in Fine and Thoroughman (2006), the authors failed to look for motion-dependent learning in their data, and several technical issues with the analysis make it difficult to interpret post hoc the actual shapes of the force patterns that they estimated to be associated with motor adaptation.

Previous work on motion-dependent learning. Foundational studies on the adaptive responses to novel environmental dynamics employed perturbations that were directly dependent on limb motion—for example, linear velocity-dependent FFs (Shadmehr and Mussa-Ivaldi 1994) or Coriolis force perturbations in a rotating room (Lackner and Dizio 1994). Both types of studies demonstrated that subjects readily adapted to these perturbations, suggesting that the motor system might have a special proclivity for learning motion-dependent dynamics. However, these studies failed to address whether the velocity-dependent dynamics were specifically learned in a motion-dependent fashion; consequently, their results could be explained by a general ability to adapt to arbitrary perturbations. A pair of studies by Conditt and Mussa-Ivaldi then showed that the adaptation to velocity-dependent FFs or close approximations of them generalized in a velocity-dependent manner to untrained movement trajectories (Conditt et al. 1997; Conditt and Mussa-Ivaldi 1999), supporting the idea that motion-dependent motor primitives underlie this type of adaptation. In line with this idea, several studies have suggested that this velocity-dependent learning extrapolates to faster, untrained movements in a linear, velocity-dependent fashion (Goodbody and Wolpert 1998; Joiner et al. 2011). Moreover, we recently found that early adaptation to position-dependent dynamics elicited an adaptive response with a seemingly inappropriate velocity-dependent component, whereas early adaptation to velocity-dependent dynamics elicited an inappropriate position-dependent component (Sing et al. 2009). This cross-adaptation indicates that the abilities to adapt to position- and velocity-dependent dynamics manifest themselves even when these dynamics are not specifically encountered.

Although the work on generalization, extrapolation, and cross-adaptation demonstrates that motion-dependent representations are formed when adapting to dynamics that are motion dependent or nearly motion dependent, it is possible that other types of representations are formed when adapting to force perturbations that are largely not motion dependent. Consequently, studies of motion-dependent dynamics may not be the strongest test of the idea that motor adaptation is intrinsically motion dependent. This is because motion-dependent dynamics would elicit motion-dependent adaptive responses that could overshadow other components of the adaptive response, even if non-motion-dependent features were specifically represented by the motor primitive population. Thus here we studied the adaptive response to force-impulse perturbations that could not be well approximated by motion-dependent representations ($R^2 < 0.19$ for both FPs we studied) and found that responses were nevertheless dominated by motion-dependent components throughout the course of adaptation. Moreover, we found that although the composition of the adaptive response evolved during training as the relative contributions of position-, velocity-, and acceleration-dependent components changed, the structure of the adaptive response did not change. This structure consisted of a linear combination of the same three motion components throughout the entire 392-trial training period that we examined and the 100-trial decay period that followed it. Correspondingly, we found that subtle trial-to-trial variations in motion predicted trial-to-trial variations in both the size and shape of the adaptive response in line with a model of motion-dependent learning.

It should be noted that a strongly nonlinear state representation in terms of position would be clearly capable of accurately approximating the position-triggered force pulses that we studied here, although linear combinations of the position, velocity, and acceleration of movement cannot. The simplest such nonlinear approximation would be a pulse-shaped representation of the perturbation based entirely on position, reflecting the lateral force typically encountered at each longitudinal position into the movement. However, such a nonlinear representation would clearly be outside of the subspace spanned by linear combinations of position, velocity, and acceleration. Therefore the finding that 96% of the variance in the shape of the average adaptive response can be explained by a simple linear combination of the position, velocity, and acceleration of motion suggests that internal representations of dynamics are not only motion dependent but motion dependent in a linear (or nearly linear) fashion. Thus the present results indicate that the primitives for motor adaptation consist primarily of linear or nearly linear functions of the position, velocity, and acceleration that are combined in an effectively linear manner. Why should this be the case? Our present findings complement earlier work on internal models of environmental dynamics, and they provide the most compelling evidence to date about the nature of the internal representations that underlie the adaptive responses to these dynamics.

GRANTS

This work was supported by grants from the McKnight Endowment for Neuroscience, the Alfred P. Sloan Foundation, and the Wallace H. Coulter Foundation to M. A. Smith.

DISCLOSURES

No conflicts of interest, financial or otherwise, are declared by the author(s).

AUTHOR CONTRIBUTIONS

Author contributions: G.C.S. and M.A.S. conception and design of research; G.C.S. and S.P.O. performed experiments; G.C.S., S.P.O., and M.A.S. analyzed data; G.C.S., S.P.O., and M.A.S. interpreted results of experiments; G.C.S., S.P.O., and M.A.S. prepared figures; G.C.S. and M.A.S. drafted manuscript; G.C.S. and M.A.S. edited and revised manuscript; G.C.S., S.P.O., and M.A.S. approved final version of manuscript.

REFERENCES

Ashe J, Georgopoulos AP. Movement parameters and neural activity in motor cortex and area 5. *Cereb Cortex* 4: 590–600, 1994.

Baraduc P, Wolpert DM. Adaptation to a visuomotor shift depends on the starting posture. *J Neurophysiol* 88: 973–981, 2002.

Bastian AJ, Martin TA, Keating JG, Thach WT. Cerebellar ataxia: abnormal control of interaction torques across multiple joints. *J Neurophysiol* 76: 492–509, 1996.

Bays PM, Wolpert DM. Actions and consequences in bimanual interaction are represented in different coordinate systems. *J Neurosci* 26: 7121–7126, 2006.

Bellman R, Åström KJ. On structural identifiability. *Math Biosci* 7: 329–339, 1970.

Downloaded from http://jn.physiology.org/ at Harvard Univ on July 1, 2013

Bhushan N, Shadmehr R. Computational nature of human adaptive control during learning of reaching movements in force fields. *Biol Cybern* 81: 39–60, 1999.

Brayanov JB, Press DZ, Smith MA. Motor memory is encoded as a gain-field combination of intrinsic and extrinsic action representations. *J Neurosci* 32: 14951–14965, 2012.

Cheney PD, Fetz EE. Corticomotoneuronal cells contribute to long-latency stretch reflexes in the rhesus monkey. *J Physiol* 349: 249–272, 1984.

Churchland MM, Afshar A, Shenoy KV. A central source of movement variability. *Neuron* 52: 1085–1096, 2006.

Cohen MR, Meissner GW, Schafer RJ, Raymond JL. Reversal of motor learning in the vestibulo-ocular reflex in the absence of visual input. *Learn Mem* 11: 559–565, 2004.

Coltz JD, Johnson MT, Ebner TJ. Cerebellar Purkinje cell simple spike discharge encodes movement velocity in primates during visuomotor arm tracking. *J Neurosci* 19: 1782–1803, 1999.

Conditt MA, Gandolfo F, Mussa-Ivaldi FA. The motor system does not learn the dynamics of the arm by rote memorization of past experience. *J Neurophysiol* 78: 554–560, 1997.

Conditt MA, Mussa-Ivaldi FA. Central representation of time during motor learning. *Proc Natl Acad Sci USA* 96: 11625–11630, 1999.

Cordo PJ. Kinesthetic control of a multijoint movement sequence. *J Neurophysiol* 63: 161–172, 1990.

Craig JJ. *Adaptive Control of Mechanical Manipulators*. Reading, MA: Addison-Wesley, 1988.

Criscimagna-Hemminger SE, Shadmehr R. Consolidation patterns of human motor memory. *J Neurosci* 28: 9610–9618, 2008.

Diedrichsen J, Criscimagna-Hemminger SE, Shadmehr R. Dissociating timing and coordination as functions of the cerebellum. *J Neurosci* 27: 6291–6301, 2007.

Duda RO, Hart PE, Stork DG. *Pattern Classification*. New York: Wiley, 2004.

Fernandez-Ruiz J, Diaz R, Aguilar C, Hall-Haro C. Decay of prism aftereffects under passive and active conditions. *Cogn Brain Res* 20: 92–97, 2004.

Fine MS, Thoroughman KA. Motor adaptation to single force pulses: sensitive to direction but insensitive to within-movement pulse placement and magnitude. *J Neurophysiol* 96: 710–720, 2006.

Friston KJ, Josephs O, Rees G, Turner R. Nonlinear event-related responses in fMRI. *Magn Reson Med* 39: 41–52, 1998.

Fu QG, Flament D, Coltz JD, Ebner TJ. Relationship of cerebellar Purkinje cell simple spike discharge to movement kinematics in the monkey. *J Neurophysiol* 78: 478–491, 1997.

Ghahramani Z, Wolpert DM, Jordan MI. Generalization to local remappings of the visuomotor coordinate transformation. *J Neurosci* 16: 7085–7096, 1996.

Gonzalez Castro LN, Monsen CB, Smith MA. The binding of learning to action in motor adaptation. *PLoS Comput Biol* 7: e1002052, 2011.

Goodbody SJ, Wolpert DM. Temporal and amplitude generalization in motor learning. *J Neurophysiol* 79: 1825–1838, 1998.

Hwang EJ, Donchin O, Smith MA, Shadmehr R. A gain-field encoding of limb position and velocity in the internal model of arm dynamics. *PLoS Biol* 1: e25, 2003.

Hwang EJ, Smith MA, Shadmehr R. Adaptation and generalization in acceleration-dependent force fields. *Exp Brain Res* 169: 496–506, 2006.

Joiner WM, Ajayi O, Sing GC, Smith MA. Linear hypergeneralization of learned dynamics across movement speeds reveals anisotropic, gain-encoding primitives for motor adaptation. *J Neurophysiol* 105: 45–59, 2011.

Joiner WM, Smith MA. Long-term retention explained by a model of short-term learning in the adaptive control of reaching. *J Neurophysiol* 100: 2948–2955, 2008.

Juang JN. *Applied System Identification*. Upper Saddle River, NJ: Prentice Hall, 1994.

Kang Y, Endo K, Araki T. Excitatory synaptic actions between pairs of neighboring pyramidal tract cells in the motor cortex. *J Neurophysiol* 59: 636–647, 1988.

Karniel A, Mussa-Ivaldi FA. Sequence, time or state representation: how does the motor control system adapt to variable environments? *Biol Cybern* 89: 10–21, 2003.

Koop G, Pesaran MH, Potter SM. Impulse response analysis in nonlinear multivariate models. *J Econometrics* 74: 119–147, 1996.

Krakauer JW, Pine ZM, Ghilardi MF, Ghez C. Learning of visuomotor transformations for vectorial planning of reaching trajectories. *J Neurosci* 20: 8916–8924, 2000.

Kutch JJ, Kuo AD, Rymer WZ. Extraction of individual muscle mechanical action from endpoint force. *J Neurophysiol* 103: 3535–3546, 2010.

Lackner JR, Dizio P. Rapid adaptation to Coriolis force perturbations of arm trajectory. *J Neurophysiol* 72: 299–313, 1994.

Lang CE, Bastian AJ. Cerebellar subjects show impaired adaptation of anticipatory EMG during catching. *J Neurophysiol* 82: 2108–2119, 1999.

Maschke M, Gomez CM, Ebner TJ, Konczak J. Hereditary cerebellar ataxia progressively impairs force adaptation during goal-directed arm movements. *J Neurophysiol* 91: 230–238, 2004.

Mattar AA, Ostry DJ. Modifiability of generalization in dynamics learning. *J Neurophysiol* 98: 3321–3329, 2007.

Mattar AA, Ostry DJ. Generalization of dynamics learning across changes in movement amplitude. *J Neurophysiol* 104: 426–438, 2010.

Miall RC, Christensen LO, Cain O, Stanley J. Disruption of state estimation in the human lateral cerebellum. *PLoS Biol* 5: e316, 2007.

Morton SM, Bastian AJ. Prism adaptation during walking generalizes to reaching and requires the cerebellum. *J Neurophysiol* 92: 2497–2509, 2004.

Morton SM, Lang CE, Bastian AJ. Inter- and intra-limb generalization of adaptation during catching. *Exp Brain Res* 141: 438–445, 2001.

Mussa-Ivaldi FA, Bizzi E. Motor learning through the combination of primitives. *Philos Trans R Soc Lond B Biol Sci* 355: 1755–1769, 2000.

Paninski L, Fellows MR, Hatsopoulos NG, Donoghue JP. Spatiotemporal tuning of motor cortical neurons for hand position and velocity. *J Neurophysiol* 91: 515–532, 2004.

Pasalar S, Roitman AV, Durfee WK, Ebner TJ. Force field effects on cerebellar Purkinje cell discharge with implications for internal models. *Nat Neurosci* 9: 1404–1411, 2006.

Poggio T, Bizzi E. Generalization in vision and motor control. *Nature* 431: 768–774, 2004.

Quaia C, Joiner WM, Fitzgibbon EJ, Optican LM, Smith MA. Eye movement sequence generation in humans: motor or goal updating? *J Vis* 10: 28, 2010.

Rabe K, Livne O, Gizewski ER, Aurich V, Beck A, Timmann D, Donchin O. Adaptation to visuomotor rotation and force field perturbation is correlated to different brain areas in patients with cerebellar degeneration. *J Neurophysiol* 101: 1961–1971, 2009.

Scheidt RA, Reinkensmeyer DJ, Conditt MA, Rymer WZ, Mussa-Ivaldi FA. Persistence of motor adaptation during constrained, multi-joint, arm movements. *J Neurophysiol* 84: 853–862, 2000.

Shadmehr R, Mussa-Ivaldi FA. Adaptive representation of dynamics during learning of a motor task. *J Neurosci* 14: 3208–3224, 1994.

Shidara M, Kawano K, Gomi H, Kawato M. Inverse-dynamics model eye movement control by Purkinje cells in the cerebellum. *Nature* 365: 50–52, 1993.

Sing GC, Joiner WM, Nanayakkara T, Brayanov JB, Smith MA. Primitives for motor adaptation reflect correlated neural tuning to position and velocity. *Neuron* 64: 575–589, 2009.

Sing GC, Smith MA. Reduction in learning rates associated with anterograde interference results from interactions between different timescales in motor adaptation. *PLoS Comput Biol* 6: e10000893, 2010.

Smith MA, Brandt J, Shadmehr R. Motor disorder in Huntington's disease begins as a dysfunction in error feedback control. *Nature* 403: 544–549, 2000.

Smith MA, Ghazizadeh A, Shadmehr R. Interacting adaptive processes with different timescales underlie short-term motor learning. *PLoS Biol* 4: e179, 2006.

Smith MA, Shadmehr R. Intact ability to learn internal models of arm dynamics in Huntington's disease but not cerebellar degeneration. *J Neurophysiol* 93: 2809–2821, 2005.

Stark E, Drori R, Asher I, Ben-Shaul Y, Abeles M. Distinct movement parameters are represented by different neurons in the motor cortex. *Eur J Neurosci* 26: 1055–1066, 2007.

Thoroughman KA, Shadmehr R. Learning of action through adaptive combination of motor primitives. *Nature* 407: 742–747, 2000.

Thoroughman KA, Taylor JA. Rapid reshaping of human motor generalization. *J Neurosci* 25: 8948–8953, 2005.

Wagner MJ, Smith MA. Shared internal models for feedforward and feedback control. *J Neurosci* 28: 10663–10673, 2008.

Wang W, Chan SS, Heldman DA, Moran DW. Motor cortical representation of position and velocity during reaching. *J Neurophysiol* 97: 4258–4270, 2007.

Wei K, Kording K. Relevance of error: what drives motor adaptation? *J Neurophysiol* 101: 655–664, 2009.

Wei K, Wert D, Kording K. The nervous system uses nonspecific motor learning in response to random perturbations of varying nature. *J Neurophysiol* 104: 3053–3063, 2010.

Downloaded from http://jn.physiology.org/ at Harvard Univ on July 1, 2013